Early-to-mid idiopathic Parkinson's disease shows a more cytotoxic but declined CD8-regulatory peripheral immune profile

Christophe Capelle
Luxembourg Institute of Health
Séverine Cire
Luxembourg Institute of Health
Maxime Hansen
University of Luxembourg
Lukas Pavelka
University of Luxembourg
Fanny Hedin
Luxembourg Institute of Health
Maria Konstantinou
Luxembourg Institute of Health
Dominique Revets
Luxembourg Institute of Health
Vera Tslaf
Luxembourg Institute of Health
Taina Marques
University of Luxembourg
Alexandre Baron
Luxembourg Institute of Health
Olivia Domingues
Department of Infection and Immunity, Luxembourg Institute of Health
Ni Zeng
Luxembourg Institute of Health https://orcid.org/0000-0003-2756-6074
Patrick May
University of Luxembourg https://orcid.org/0000-0001-8698-3770
Antonio Cosma
Luxembourg Institute of Health https://orcid.org/0000-0002-3686-8034
Rudi Balling
Luxembourg Centre for Systems Biomedicine, University of Luxembourg, Esch-sur-Alzette
https://orcid.org/0000-0003-2902-5650

Rejko Krüger
Luxembourg Institute of Health
Markus Ollert
Department of Infection and Immunity, Luxembourg Institute of Health
Feng Hefeng (feng.he@lih.lu)
Luxembourg Institute of Health https://orcid.org/0000-0003-2657-7361

Article

Keywords: Parkinson's disease, Peripheral immune system, CD8 TEMRA, CD8 regulatory T cells 27 (CD8 Treg), Systems immunology

Posted Date: July 22nd, 2022

DOI: https://doi.org/10.21203/rs.3.rs-1834770/v1

Early-to-mid idiopathic Parkinson's disease shows a more cytotoxic but declined CD8-regulatory peripheral immune profile

Christophe M. Capelle[1, 2], Séverine Ciré[1], Maxime Hansen[3, 4], Lukas Pavelka[3, 4], Fanny Hedin[5], Maria Konstantinou[5], Dominique Revets[5], Vera Tslaf[1, 2, 6], Tainá Marques[3], Alexandre Baron[1], Olivia Domingues[1], Ni Zeng[1 ,2], Patrick May[3], Antonio Cosma[5], Rudi Balling[3,7], Rejko Krüger[3, 4, 6], Markus Ollert[1, 8], Feng Q. Hefeng[1 *]

[1] Department of Infection and Immunity, Luxembourg Institute of Health (LIH), 29, rue Henri Koch, L-4354, Esch-sur-Alzette, Luxembourg

[2] Faculty of Science, Technology and Medicine, University of Luxembourg, 2, avenue de Université, L-4365, Esch-sur-Alzette, Luxembourg

[3] Luxembourg Centre for Systems Biomedicine (LCSB), University of Luxembourg, 6, avenue du Swing, L-4367, Belvaux, Luxembourg

[4] Parkinson Research Clinic, Centre Hospitalier de Luxembourg (CHL), 4, Rue Nicolas Ernest Barblé, L-1210, Luxembourg, Luxembourg

[5] National Cytometry Platform, Luxembourg Institute of Health, 29, rue Henri Koch, L-4354 Esch-sur-Alzette, Luxembourg

[6] Transversal Translational Medicine, Luxembourg Institute of Health, 1A-B, rue Thomas Edison, L-1445, Strassen, Luxembourg

[7] Institute of Molecular Psychiatry, University of Bonn, Venusberg-Campus 1, D-53127, Bonn, Germany

[8] Department of Dermatology and Allergy Center, Odense Research Center for Anaphylaxis (ORCA), University of Southern Denmark, Odense, 5000 C, Denmark

* Corresponding author. Direct correspondence to feng.he@lih.lu

Running title: Disturbed peripheral immune system in early-to-mid iPD

Keywords: Parkinson's disease; Peripheral immune system; CD8 TEMRA; CD8 regulatory T cells (CD8 Treg); Systems immunology.

Abstract

Parkinson's disease (PD) is the second most common neurodegenerative disease. Brain neuroinflammation plays a role in PD pathogenesis. However, the involvement of the peripheral immune system has not been systematically investigated. Here we analyzed >700 combinatorial immunological features in fresh blood of 28 early-to-mid-stage PD patients and 24 matched controls. We found an enhanced cytotoxic immune profile in idiopathic PD patients (iPD), with a higher frequency of terminally-differentiated effector CD8 T (TEMRA), late-differentiated $CD8^+$ natural killer T cells and neutrophils. This immune profile was intensified by elevated serum granzyme A, reduced percentages of $CD8^+FOXP3^+$ regulatory T cells and group 2 innate lymphoid cells with immunosuppressive or tolerance-inducing functions. The frequency of CD8 TEMRA was negatively correlated with disease duration, suggesting a contribution to PD pathogenesis. Our work provides a comprehensive map on disturbed peripheral adaptive and innate immune cells in early-to-mid iPD, proposing easily-accessible candidates for early diagnosis and treatments.

Introduction

Parkinson's disease (PD) is the second most common neurodegenerative disease after Alzheimer's disease (AD), affecting around 10 million people worldwide (Dorsey et al. 2007, Poewe et al. 2017). In addition to the neuron-autonomous mechanisms, activated microglia and neuro-inflammation in the brain of PD patients are also implicated in the pathogenesis of PD (Wang et al. 2015). At the same time, PD patients are characterized by altered levels of several circulating cytokines (Reale et al. 2009, Qin et al. 2016). Moreover, targeted studies of selected immune cells in the peripheral blood of participants found a reduction of CD4 T cells in PD patients versus healthy controls (Jiang et al. 2017). Not only total CD4 T cells, but also specific CD4 subsets, such as CD4 regulatory T cells (Treg), Th1 or Th17 (Kustrimovic et al. 2018, Sommer et al. 2018), have shown changes in PD patients. Nevertheless, the role of various CD4 subsets demonstrated in different cohorts is still controversial (Storelli et al. 2019). These inconsistent results urge the need to be further clarified.

Emerging evidence strongly suggests the involvement of peripheral CD8 T cells in other neurodegenerative diseases, e.g., in Alzheimer's disease (Gate et al. 2020). In PD, cytotoxic CD8 T-cell infiltration has been reported in post-mortem brain tissues even before the α-synuclein (α-syn) aggregation and neuronal death, suggesting a potential role of CD8 T cells in initiating PD pathology (Galiano-Landeira et al. 2020). In addition, α-syn-specific T cells have been reported in the peripheral blood of PD patients (Sulzer et al. 2017) and were associated with pre-clinical and early PD (Lindestam Arlehamn et al. 2020). In a genetic-PD mouse model, the cytotoxic CD8 T-cell response against mitochondrial antigens caused PD-like motor symptoms (Matheoud et al. 2019). Another PD familial gene, LRRK2, regulates inflammation during infection of an animal model (Shutinoski et al. 2019). We have recently shown that another key familial PD gene, DJ-1/PAKR7, also acts on T-cell compartments, as demonstrated in both human subjects and old mice (Zeng et al. 2022), by playing a causative role in regulating the peripheral immunoaging process (Deleidi et al. 2015), which might further contribute to the pathogenesis of PD. However, it still remains unknown whether any specific subset of T cells and/or other peripheral immune cells contribute to the pathogenesis of idiopathic PD (iPD), i.e., PD without a defined genetic risk. Since most PD cases cannot be associated with a genetic origin, it is burning to identify potential novel factors leading to iPD, such as disturbed peripheral immune signatures.

Although one immune cell type usually acts in a coordinated fashion with other immune or stromal cells (Davis et al. 2017, Delhalle et al. 2018), most aforementioned studies investigating the peripheral immune system in PD have so far focused on the analysis of a few selected immune subsets following predefined hypotheses. Those hypothesis-driven studies cannot identify previously-unrecognized changes. Though a recent study has used unbiased single-cell RNA-seq analysis (Wang et al. 2021), that analysis was restricted to T cells. Furthermore, the conclusions of

that study were compromised by a very low, single-digit number of included PD patients and the lack of disease stage information. Meanwhile, the biomedical research community is still desperately seeking for easily-accessible validated peripheral cellular or molecular biomarkers that allow for the early diagnosis of PD [as reviewed here (Emamzadeh and Surguchov 2018, Parnetti et al. 2019)]. To address these challenging questions and unmet clinical needs, we applied a systems-immunology approach to comprehensively analyze the peripheral immune system of early-to-mid stage PD patients and matched healthy controls (HC). By focusing on early-to-mid stage patients, we reasoned to have a higher probability to identify the peripheral immune cells that drive the initiation of the pathogenesis of PD, especially of iPD, rather than those responding secondary to the manifestation of pathological events in PD.

Results

Single-cell CyTOF analysis shows a more-cytotoxic and late-differentiated immune profile in early-to-mid stage iPD

In this study, we systematically analyzed various immune subsets and their functional states in 28 PD patients (25 iPD aged 60-70 years and three genetic PD patients with mutations in GBA or PINK1) and 24 matched healthy controls (HC) (refer to “cohort design” in **Materials and Methods**, **Table S1** and **S2** for more details; for simplicity, ‘PD patients’ were shortened as PD hereafter). This was realized by investigating 37 different innate and adaptive immune subsets and more than 700 combinatorial T-cell features, using a 35-marker mass cytometry (also known as Cytometry by Time of Flight or CyTOF) panel and five panels of multiple-color flow-cytometry (FCM) composed of 33 lineage and functional T-cell markers, respectively (**Figure 1**, **2A**, **Table S3** and **S4**). We recruited the participants from the ongoing nation-wide Luxembourg Parkinson’s study with more than 800 PD and 800 HC (Hipp et al. 2018) (https://parkinson.lu/research-participation/luxembourg-parkinsons-study) and controlled for several major confounding factors, medications and comorbidities, known to affect the immune system, to ensure that our observations are PD-specific (for details, refer to **Figure 1** and **Table S1**). Furthermore, we narrowed the patients to those with early-to-mid stage disease [Hoehn and Yahr (H&Y) staging scale: mean=2.3, ranging from 1.5 to 3.0; most of them were ≤2.5, except for five participants with a scale of 3] and with a disease duration of less than 10 years (except for three patients with a duration of 12, 13 or 19 years).

As a strong cryopreservation effect has been observed on the FCM readouts of several clinically-relevant T-cell markers in bio-banked samples (Capelle et al. 2021), we performed the CyTOF analysis on fresh whole blood of PD and HC (for gating strategy refer to **Fig. S1**). A principle component analysis (PCA) showed that PD did not have a distinct immunological fingerprint based

on the entire peripheral immune system (**Figure 2B**). Nevertheless, several immune cell types were altered in PD compared to HC, in particular in the T-cell compartment (**Figure 2C**). Total classical αβ T cells were modestly reduced in PD (**Fig. S2A**), reflected by a decrease of total CD4 T cells (**Fig. S2B**), whereas the γδ T cells were unchanged among total living $CD45^+$ cells (**Fig. S2C**). The frequency among living $CD45^+$ cells well recapitulated the absolute number of cells for the given subset as we standardized the amount of analyzed whole blood from each participant and no difference in the number of total living $CD45^+$ cells was observed between PD and HC (refer to Materials and Methods, **Table S5**). The decreased frequency of total CD4 T cells among living $CD45^+$ cells was mainly due to a decrease in $CD4^+CXCR5^+$ T follicular helper cells (Tfh) (**Fig. S2D**), $CD45RA^+CCR7^+$ naïve (**Fig. S2E**) and $CD45RA^-CCR7^+$ central memory (TCM) $CD25^-$ conventional T cells (Tconv) among total living $CD45^+$ immune cells (**Fig. S2F**), but not $CD45RA^-CCR7^-$ effector memory (TEM) Tconv (**Fig. S2G**). Although total CD8 T cells showed no difference in PD (**Figure 2D**), the CD8 naïve/memory subset composition displayed alterations (**Figure 2C**). As demonstrated by an unbiased volcano plot analysis (**Figure 2C**), the frequency of cytotoxic terminally-differentiated effector T cells ($CD45RA^+CCR7^-$, TEMRA) (Pereira and Akbar 2016, Goronzy and Weyand 2017) was substantially increased among total CD8 T cells in PD (**Figure 2C, E**), whereas the frequency of TCM cells was reduced (**Figure 2F**). The proportion of CD8 naïve and TEM cells showed similarity between PD and HC (**Fig. S2H, I**). Furthermore, the expression of CD57, a marker of terminal differentiation, among CD8 TEMRA showed a trend to be increased ($p=0.066$) in PD (**Figure 2G**), further indicating a more-differentiated CD8 T-cell profile. Moreover, another cytotoxic cell type, natural killer T (NKT) cells also exhibited a late-differentiated state, as reflected by an increased frequency of $CD8^+$ NKT (**Figure 2H**) among total NKT cells (Liu et al. 2019), while the frequency of less-differentiated $CD4^+$ (**Figure 2I**) and $CD4^-CD8^-$ (also known as double negative, **Figure 2J**) NKT cells was either decreased or intact, respectively. Similar to CD8 T cells, $CD8^+$ NKT also expressed higher levels of CD57 (**Figure 2K**). Consistent with the accelerated-differentiation notion, the frequency of $CD56^{high}CD57^-$ immature NK cells was decreased among total living $CD45^+$ cells (**Figure 2L**). As the CD8 T-cell composition was considerably changed, while total CD8 T cells were intact, we performed an unsupervised analysis on gated CD8 T cells to substantiate our supervised analysis. Indeed, a viSNE plot analysis confirmed an enhanced frequency of CD8 TEMRA ($CD45RA^+CCR7^-CD27^-$) among total CD8 T cells in PD versus HC (**Figure 2M**). To sum up, we observed a more-cytotoxic and late-differentiated immune profile in early-to-mid iPD, as reflected by the changed frequency of several relevant cell types, such as CD8 TEMRA, NKT and NK cells.

With the 35-marker CyTOF analysis, we were also able to assess many other immune subsets, such as granulocytes (neutrophils, eosinophils and basophils), monocytes (classical, intermediate and non-classical), dendritic cells (myeloid DC and plasmacytoid DC, known as mDC and pDC respectively), NK (immature and late), B cells (naïve, memory, plasma cells) and innate lymphoid

cells (ILCs: ILC1, ILC2 and ILC3) (**Fig. S1** and **Table S5**). Most of them did not show any significant change in PD versus matched HC in terms of the frequency among total CD45+ cells or the frequency among the relevant parent gates (**Table S5**). Consistent with a more-cytotoxic profile, an increased frequency of neutrophils among living $CD45^+$ cells was observed in PD (**Figure 2N**). The heightened frequency of neutrophils was accompanied by a reduced fraction of eosinophils (**Figure 2O**), while basophils were unchanged in PD (**Fig. S2J**). The reduced frequency of eosinophils is concordant with the observation showing a negative association between eosinophils and the risk of PD in a study based on routine whole-blood counts (Wang et al. 2021). Our finding regarding neutrophils is also in agreement with a recent study only analyzing whole-blood-count parameters (Munoz-Delgado et al. 2021).

Unexpectedly, the frequency of ILC2 (Moro et al. 2010) among total living $CD45^+$ immune cells in PD was almost decreased to half of that in matched HC (**Figure 2P, Q**), while ILC1 and ILC3 showed no difference (**Fig. S2K, L**). These data are aligned with the observed decrease in eosinophils, as ILC2 control eosinophil homeostasis, at least in the context of typical Th2 immunopathology, i.e., allergy (Nussbaum et al. 2013). Finally, we found a slight but significant decrease in the frequency of IgD^+CD27^- naïve B cells (**Fig. S2M**). Collectively, our unbiased comprehensive immunophenotyping analysis revealed a more-cytotoxic and late-differentiated immune profile while the frequency of immature NK cells, eosinophils and ILC2 was significantly decreased in early-to-mid stage PD.

Early-to-mid iPD exhibited an increased effector profile in CD8 T cells

Since our CyTOF analysis has shown substantial alterations within T-cell compartments in whole blood of PD, we next analyzed T cells in more depth using five FCM panels with a total of 33 T cell-relevant markers, the combinations of which gave rise to ~700 features. In this way, we were able to assess not only phenotypical markers and the proportions of different T cell subpopulations, but also functional states of different subsets (**Table S4**). The PCA based on ~700 different combinations determined a distinct immunological fingerprint in PD compared to HC (with the exception of one PD and one HC participant labelled as “PD9” and “HC17” in **Figure 3A**). The three genetic PD were not identified as outliers compared to iPD patients in the PCA plot based on the comprehensive T-cell analysis. Alike to the CyTOF data, no difference was observed in the frequency of total CD8 T cells among peripheral blood mononuclear cells (PBMC) in PD versus HC (**Fig. S3A**). Different from the CyTOF data, we did not observe any significant difference in the frequency of total T cells and total CD4 T cells between the two groups (**Fig. S3A**). The unchanged frequency of total T cells revealed by our FCM analysis might be due to the exclusion of granulocytes in PBMC, accounting for the majority of the immune population in whole blood. Although the overall frequency of major T-cell populations remained statistically unchanged in the FCM analysis (**Fig. S3A**), a PCA analysis

revealed a clear T-cell fingerprint in PD, reflecting the changes in specific T-cell subsets (**Figure 3A**).

Among the most significantly changed ($p<0.05$, fold change >1.4) immune subpopulations in PD, the FCM analysis again found a strong increase in the frequency of TEMRA among total CD8 T cells (**Figure 3B, C**), independently confirming our CyTOF results. CD8 TEMRA cells express CD45RA, but lose the expression of CD45RO, CCR7 and CD27. By analyzing the expression of CCR7 in combination with CD45RA and CD45RO, we were able to better differentiate the CD8 subpopulations and pinpointed that $CD45RA^+CD45RO^-CCR7^-$ cells (CD8 TEMRA following a simplified gating strategy) were increased among total CD8 T cells in PD (**Figure 3C**).

To more strictly identify CD8 TEMRA, we next included CD27 in another staining panel. In line with the results based on the simplified gating strategy aforementioned (**Figure 3C**), the frequency of $CD45RO^-CCR7^-CD27^-$ effector CD8 T cells was also increased in PD (**Fig. S3B**). Based on the fact that the fraction of CD45RA/CD45RO double-negative (mean: ~5%) or double-positive (mean: ~5%) cells was tiny among CD8 T cells (**Fig. S3C**), most of the $CD45RO^-CCR7^-CD27^-$ effector CD8 T cells (**Fig. S3B**) should be $CD45RA^+CCR7^-CD27^-$ CD8 TEMRA. Meanwhile, TCM ($CD45RO^+CCR7^+CD27^+$) and transitional memory (TM) ($CD45RO^+CCR7^-CD27^+$) CD8 T cells were reduced (**Fig. S3D, E**), while naïve ($CD45RO^-CCR7^+CD27^+$) CD8 T cells showed no difference between PD and HC (**Fig. S3F**). The reduction in CD8 TCM and TM cells was in line with a lower frequency of long-lived memory ($KLRG1^-CD127^+$) (Kaech et al. 2003) CD8 T cells (**Fig. S3G**) and consistent with the CyTOF results (**Figure 2F**). Collectively, we firmly demonstrated that the portion of CD8 TEMRA was increased while the CD8 TCM/TM fraction was contracted among early-to-mid stage PD, no matter which gating strategies were employed in various staining panels based on both multi-channel FCM and CyTOF approaches.

We next investigated the functional states of various T cell subsets. T-bet is an essential marker for effector CD8 lymphocyte functions (Sullivan et al. 2003, Intlekofer et al. 2005) and its expression is positively correlated with GZMB expression in humans infected with cytomegalovirus (CMV) (Popescu et al. 2014). In line with the notion of the increased effector profile, CD8 T cells from PD compared to HC also displayed a higher frequency of $T\text{-bet}^{high}$ and $CD45RO^-T\text{-bet}^+$ CD8 T cells (**Figure 3D-E**). It is worthy to note that the $T\text{-bet}^+$ or $T\text{-bet}^{high}$ cells were mainly $CD45RO^-$, but not $CD45RO^+$ cells, indicating that those cells were mostly $CD45RA^+$ terminally-differentiated cells, based on the largely mutually exclusive relationship between CD45RA and CD45RO expression (**Fig. S3B**). The increased CD8 effector function was further consolidated by an augmented proliferation and activation levels among $CD45RO^-$ CD8 T cells, as quantified by the expression of Ki67 (**Figure 3F**) and HELIOS (Akimova et al. 2011) (**Figure 3G**), respectively. The increase of $CD45RO^-CD57^+$ (**Figure 3H**) and $CD57^+$ (**Fig. S3H**) among CD8 T cells further supported an

advanced differentiation state of CD8 T cells in PD, as the expression of CD57 increases during CD8 T-cell differentiation (Strioga et al. 2011).

We further analyzed whether CD8 T cells from PD show any exhausted (Yi et al. 2010, Wherry 2011), senescence (Chou and Effros 2013, Lee et al. 2016) or other key dysfunctional phenotypes as the participants in our cohort were aged over 60 years old. Assessing the expression of several key T-cell exhaustion markers such as PD-1, CTLA4 and LAG3 showed no sign of exhaustion (**Fig. S3I-K**). Similar to the exhaustion scenario, the CD8 T cell senescence marker KLRG1 was unchanged between PD and HC (**Fig. S3L**). Interestingly, the activation marker ICOS was significantly decreased in CD8 T cells of PD (**Fig. S3M**). However, this decline only reflected the observed decrease in the frequency of CD8 TCM cells (**Fig. S3D**), as only the frequency of $ICOS^+CD45RO^+$, but not of $ICOS^+CD45RO^-$ CD8 T cells was decreased (**Fig. S3N**). We also observed a decreased expression of the amino acid transporter CD98 (**Fig. S3O**), nevertheless, being independent of the fraction of $CD45RO^+$ ones among CD8 T cells (**Fig. S3P**). Together, these observations support the notion that CD8 T cells in early-to-mid PD exhibited a terminally-differentiated but non-exhausted and non-senescent state.

Effector CD8 T cells tend to migrate to non-lymphoid tissues where an active immune response takes place (Galkina et al. 2005, Woodland and Kohlmeier 2009). Therefore, we also assessed the expression of several lymphocyte-relevant chemokine receptors, such as CXCR3, CCR4 and CCR6. In the blood of PD, we observed a lower frequency and expression levels (geometric mean, MFI) of CXCR3 and CCR4 among total CD8 T cells, whereas CCR6 showed no difference (**Fig. S4A, B**). The decrease in CXCR3 and CCR4 expression might be attributable to the decline in the frequency of TCM cells among total CD8 T cells (**Fig. S3D**), since among all the four subsets, CD8 TCM cells displayed the highest expression levels of these two chemokine receptors (**Fig. S4C**). In addition to the decrease in individual chemokine receptors, the frequency of CCR4 and CCR6 co-expressing cells was also decreased (**Fig. S4D**), although the cells expressing both receptors was sparse among total CD8 T cells (<1% in average). Accordingly, the frequency of cells lacking all the tested three chemokine receptors (CXCR3, CCR4 and CCR6) was increased among total CD8 T cells in PD versus HCs (**Fig. S4D**). We further asked whether CD8 TEMRA express one of the major homing receptors to allow them to properly migrate to the central nervous system (CNS). Since integrin alpha 4 (also known as CD49d) is the major brain homing factor of peripheral CD8 T cells controlling trafficking of CD8 T cells into the CNS (Yednock et al. 1992, Sasaki et al. 2007), we analyzed CD49d expression in CD8 T cells. However, we did not find any significant difference in CD49d expression between PD and HC among various subsets of CD8 T cells, including CD8 TEMRA (**Fig. S4E**). In brief, the unaffected expression levels of the analyzed chemokine receptors and major brain homing factor among CD8 TEMRA indicate that CD8 TEMRA have an intact potential to migrate into the CNS.

Since those cells displaying cytotoxic functions, such as CD8 T cells and NKT, also secrete cytotoxic effector molecules, we asked whether a more cytotoxic state was already reflected in the sera of PD. To this end, we measured two of the most abundant extracellular cytotoxic effector molecules, granzyme A (GZMA) and granyzme B (GZMB) together with the membrane-pore forming molecule perforin. Highly encouragingly, GZMA was significantly elevated in PD (**Figure 3I**), while the levels of both GZMB and perforin were comparable between PD and HC (**Figure 3J, K**). In short, our cellular and serological data together suggested a more-cytotoxic immune milieu in PD.

Although naïve CD4 cells displayed no difference, the frequency of CD4 TCM cells were slightly, but significantly decreased (**Fig. S5A, B**). Moreover, the portion of intermediate CD4 ($CCR7^-$ $CD27^+CD45RO^-$) (Knox et al. 2014) T cells were increased in PD (**Fig. S5C**). Unlike CD8 T cells, the frequency of effector and TEMRA among total CD4 T cells remained unchanged in PD (**Fig. S5D, E**). In short, CD8 T cells, but not CD4 T cells, favored a terminally-differentiated effector program over the generation of a long-lived CD8 central memory T-cell profile in PD.

The combination of the chemokine receptors, such as CXCR3, CCR4 and CCR6 can be also used to distinguish the CD4 T helper cell lineages Th1, Th2 and Th17 (refer to the gating strategy in **Fig. S5F**). By applying this analysis and also assessing the expression of the CD4 Th master transcription factors T-bet, GATA3 and RORγT, we observed neither a significant change in the frequency of Th1, Th2 or Th17 cells, nor in the ratios of Th subsets in PD versus HC (**Fig. S5G-J**). No change in any T helper subset was also in agreement with our CyTOF results (**Table S5**). In line with this notion, we also did not observe any significant difference in the Th1 and Th2 cytokines, such as GM-CSF, IFN-γ, IL-5 and IL-13 measured in the sera of our cohort (**Fig. S5K**). Since IL-33 plays a crucial role in regulating the ILC2 response and serves as an alarmin in the central nervous system (Cayrol and Girard 2014), we also quantified the circulating IL-33 level, which did not differ between PD and HC (**Fig. S5K**). We further measured several CNS-homing relevant chemokines, such as IL-8, IP10 and MCP-1. None of them showed any significant difference between PD and HC in our cohort (**Fig. S5K**). In short, these results indicate that the major components of the machinery enabling CD8 TEMRA to cross blood-brain barriers were not compromised in early-to-mid PD.

Together, our T-cell deep immunophenotyping analysis also firmly suggests that early-to-mid stage PD displayed a more-cytotoxic profile, characterized by a higher abundance of functional and terminally-differentiated effector CD8 T cells endowed with intact brain-homing machinery.

Early-to-mid iPD display a reduced frequency of CD8 Treg but not CD4 Treg

CD4 regulatory T cells (CD4 Treg) play an important role in suppressing effector T-cell responses to avoid an overshooting immune reaction that could harm surrounding self-tissues (Sakaguchi et al. 2008, Josefowicz et al. 2012, Schmidt et al. 2012). CD4 Treg have been found to be dysfunctional or reduced in numbers in multiple autoimmune diseases. Previous reports have shown a reduced

frequency of CD4 Treg and/or an impaired suppressive capability of Treg in PD and other neurodegenerative diseases as described or reviewed elsewhere (He and Balling 2013, Kustrimovic et al. 2018, Thome et al. 2021). Through our FCM analysis based on fresh PBMCs, we did not observe any change in the frequency of $CD4^+FOXP3^+$ T cells (CD4 Treg) among CD4 T cells between PD and HC (**Figure 4A**). Unexpectedly, we found that the frequency of $CD8^+FOXP3^+$ Treg (CD8 Treg) was reduced in PD (**Figure 4B, C**). CD8 Tregs are able suppress the responses of other effector cells, including CD8 cells [reviewed here (Kiniwa et al. 2007, Churlaud et al. 2015, Zhang et al. 2018)]. In line with our observation of reduced CD8 Treg, the expression of other markers related to CD8 Treg, such as CD25 (IL2RA) and CD122 (IL2RB) (Li et al. 2014), was also reduced in CD8 T cells of PD compared to HC (**Figure 4B**). Notably, the ratio between the frequency of CD8 TEMRA and of CD8 Treg was increased in PD versus HC, with a mean of 68.58 in PD versus 30.37 in HC, further highlighting an effector-biased, and consequently more 'active' CD8 T-cell compartment (**Figure 4D**). Although the frequency of CD4 Treg was unchanged in our PD, this data alone could not exclude the possibility of a compromised suppressive function of CD4 Treg in PD. Therefore, we also analyzed the expression of several functional markers, such as CD45RO and phospho S6 [reflecting mTORC1 activity (Zeng et al. 2013)]. Interestingly, the expression of both CD45RO and pS6 was decreased among CD4 Treg in PD (**Figure 4E**). Despite the reduction in those markers, the expression of FOXP3 and CTLA4, which are decisive for maintaining suppressor function (Schmidt et al. 2012), remained unchanged among CD4 Treg (**Figure 4F**). These data together indicate that it is mainly CD8 Treg cellularity that was impaired in early-to-mid iPD, whereas the CD4 Treg frequency and suppressive capacity were likely not affected.

CD8 TEMRA is a valuable peripheral cellular marker for early diagnosis of iPD

Considering the substantial difference in CD8 TEMRA between PD and HC in our cohort, we evaluated the potential of using CD8 TEMRA as a peripheral cellular diagnostic biomarker. We first analyzed the possible correlation between the frequency of CD8 TEMRA and various available quantitative clinical information, such as age, disease duration, H&Y staging scale, UPDRS-III (Unified Parkinson's Disease Rating Scale III), LEDD (Levodopa equivalent daily dose) and MOCA (Montreal Cognitive Assessment). Although no significant correlation was observed between CD8 TEMRA and most of those clinical data, notably, the frequency of CD8 TEMRA in PD showed a significant negative correlation with disease duration from the onset of initial symptoms (**Figure 5A**) and also a trend to be negatively correlated with the disease duration after clinical diagnosis ($p=0.054$, **Figure 5B**). This suggests that CD8 TEMRA populations might be more involved in the early rather than the later stage of PD. Interestingly, samples from early-to-mid stage PD could be already well distinguished from HC samples with an area under the curve (AUC) of 0.7731, based on CD8 TEMRA frequency alone (**Figure 5C**). As the frequency of CD8 TEMRA negatively

correlated with disease duration, we applied another receiver operating characteristic (ROC) analysis by focusing on patients diagnosed only within 5 years. Notably, an excellent AUC value of 0.8663 [for the definition of AUC ranges, refer to the seminal work (Mandrekar 2010); sensitivity of 100% and specificity of 70.83% at the cut-off of 40.3% for CD8 TEMRA percentages among CD8] was obtained based on the CD8 TEMRA frequency of those patients (**Figure 5D**).

Since the frequency of CD8 Treg and ILC2 also showed a difference between PD and HC, we assessed whether those subsets can provide additional power by analyzing them with CD8 TEMRA together in the same plots (**Figure 5E, F**). As the ratio between CD8 TEMRA and CD8 Tregs might represent the CD8 effector potential in the given individual, we also analyzed the diagnostic value by integrating the ratios with the absolute frequency of CD8 TEMRA together (**Figure 5G**). Interestingly, neither the frequency of CD8 Tregs, the frequency of ILC2 nor the ratios between CD8 TEMRA and CD8 Tregs can substantially increase the potential of implementing CD8 TEMRA as a biomarker, always leaving six out of the seven HC samples mixed in the 'PD area' (**Figure 5G**). Surprisingly, a detailed analysis into the plot displaying the ratios between CD8 TEMRA and CD8 Tregs versus the frequency of CD8 TEMRA revealed that six out of the seven 'indistinguishable' HC samples were all from males. Noticing this potential gender bias, we performed another ROC analysis using only female samples. Very encouragingly, an outstanding AUC value [for the range of outstanding AUC values, also refer to (Mandrekar 2010)] as high as 0.925 was achieved (**Figure 5H**). In short, our data firmly support that CD8 TEMRA alone might represent an unrecognized reliable easily-accessible cellular marker for early diagnosis of PD, especially for female iPD.

Discussion

It has been postulated that PD pathology might arise in the periphery and migrate to the CNS via the vagus nerve (Braak et al. 2003). More recently, Kipnis and colleagues lifted the misconception around the immune privilege in the brain (Louveau et al. 2015), making the peripheral immune system a reasonable suspect contributing to the development of neurodegenerative diseases. Here we showed that early-to-mid stage iPD displayed a highly-functional peripheral effector immune profile, as reflected by several types of more-cytotoxic and late-differentiated immune subsets, especially CD8 TEMRA. These cytotoxic CD8 T cells did not display any impairment in the expression of major chemokine receptors and brain homing factors in PD. The CD8 TEMTA frequency negatively correlated with the disease duration from the onset of initial symptoms or diagnosis. This suggests that CD8 TEMRA could be a driver of initiating PD instead of a secondary consequence following PD advancement. In support of our observations, CD8 T cells have been found to infiltrate into the CNS, prior to the onset of α-syn neuropathology and their density correlated with neuronal cell death, although in PD post-mortem brain tissues (Galiano-Landeira et al. 2020).

Thus, our data strongly support that the peripheral immune system, especially CD8 TEMRA, might contribute to PD pathogenesis, indicating that CD8 TEMRA could serve as a potent easily-accessible target to prevent the progression of iPD. However, this intervention would only be possible during a short time window early in PD, as advised by the negative correlation of TEMRA with the disease duration. Our work also suggests that peripheral CD8 TEMRA alone might be a valuable cellular peripheral non-invasive biomarker for early diagnosis, especially for female iPD.

The elevated immune cytotoxic profile of CD8 T cells and $CD8^+$ NKT cells in PD observed in our cohort might also explain why patients with PD are better protected against some, although not all, cancers (Inzelberg and Jankovic 2007). An increased number of NK cells, another type of specific cytotoxic cells, has been reported in PD through a meta-analysis (Jiang et al. 2017), further indicating that the general immune status of PD is primed towards cellular immunity. In line with that, a reduced frequency of $CD56^{high}CD57^-$ immature NK cells was observed in our cohort, indicative of a more-differentiated stage of NK cells. The cytotoxic immune profile was further supported by our observation about the enhanced frequency of neutrophils. In the meantime, the critical cytotoxic effector molecule GZMA was significantly elevated in the sera of our PD cohort, further indicating a more-cytotoxic peripheral profile in early-to-mid stage iPD. Coincidently, the frequency of hippocampal CD8 T cells producing GZMA in patients with Alzheimer's disease has also been found higher than that of the analyzed controls (Gate et al. 2020). Interestingly, extracellular GZMA has been recently reported to also play a critical pro-inflammatory role, independent of its cytotoxic function, under various pathological conditions (Metkar et al. 2008, van Daalen et al. 2020). With this in mind, our data not only strongly suggest a more-cytotoxic peripheral immune milieu, but might also indicate a pro-inflammatory-biased state in early-to-mid stage iPD.

While our PD displayed a more-cytotoxic immune profile, we also observed a reduced frequency of several regulatory cell types, known to play immune suppressive or tolerance-inducing roles. Previous studies have reported reduced CD4 Treg numbers or a decreased suppressive capability of CD4 Treg in PD (Saunders et al. 2012, Kustrimovic et al. 2018, Thome et al. 2021). However, our work provides the first evidence showing a reduced frequency of CD8 Treg in PD. CD8 Treg also play a critical role in suppressing CD8 responses and effector functions of other immune cell types (Correale and Villa 2010, Li et al. 2014, Flippe et al. 2019). Therefore, our observation suggests that a reduced frequency of CD8 Treg might fail to properly control the expansion or differentiation balance of terminally-differentiated CD8 T cells, leading to a dominant profile of cytotoxic effector CD8 T cells, which thus could contribute to the pathogenesis of iPD. It is also worthy to note that the ILC2 frequency showed the strongest decrease in PD of our cohort. Since IL-10-producing ILC2 play a critical regulatory role in the induction of immune tolerance (Golebski et al. 2021), the reduced frequency of peripheral ILC2 in our cohort might also contribute to the enhanced frequency of CD8 TEMRA in PD. Meanwhile, ILC2 also produce type 2 cytokines such as IL-5 and IL-13 (Spits and Di

Santo 2011, Hoyler et al. 2012), which in turn promote a M2-like polarization of brain-resident microglia. In line with this, infiltration of ILC2 into choroid plexus in an animal model of Alzheimer's disease enhanced the cognitive function in aged mice (Fung et al. 2020). The relationship between peripheral and CNS-residing ILC2 in PD merits further investigation, as ILC2 are the most prevalent ILC subset within the adult mouse CNS (Russi et al. 2015).

One recent single-cell RNA-seq analysis focusing on sorted T cells and TCR repertoire has reported enriched terminal effector CD8 T cells in PD, but only analyzed a single-digit number of patients (Wang et al. 2021). Furthermore, that study has neither provided information on the disease stage nor on other relevant clinical metadata, making a direct comparison of their results with ours difficult. Another study (Williams-Gray et al. 2018), similar to ours, also did not observe any major changes within CD4 T cells. However, in contrast to the single-cell RNA-seq study and ours, that study showed a reduced frequency of CD8 $CD57^{+}$ T and CD8 TEMRA cells in the peripheral blood of PD (Williams-Gray et al. 2018). The differences between their observations and ours might be attributable to very different inclusion/exclusion criteria. In that study, a wider range of patients aged between 55 and 80 years old were included, while we focused on a strictly-controlled and very-homogeneous group of patients and healthy controls, covering a more narrow age range (60-70 years old for idiopathic patients). The age range of study participants has a major impact on the immune system and on immunological parameters (Weng 2006, Goronzy and Weyand 2013). Furthermore, we controlled for the CMV-related immune status of all included participants in our analysis, as CMV is documented to drive the immune ageing process (Koch et al. 2007). Additionally, we excluded PD and HC with cancer as potential participants, which was also not specified in that study, as local responses in the tumor microenvironment and peripheral immune disturbances are common in cancer patients (Hiam-Galvez et al. 2021). These three important factors might already well explain the seemingly-contradictory observations between the different studies.

Collectively, our study provided a comprehensive peripheral immune map for early-to-mid iPD patients. Although our immunological analysis was only applied to a homogenous group of 28 PD and 24 age-matched healthy controls, we started our selection from >800 PD and >800 controls from an ongoing nation-wide cohort. Furthermore, the final number of included participants for deep immunophenotyping is comparable to other high-standard resource studies in the neuro-immunological field (Gate et al. 2020). Considering that a systematic immune profiling was even rarely performed in general healthy controls at such an advanced age, our data in healthy controls alone could also serve as an immunological cell reference for various age-related diseases. We discover that early-to-mid stage iPD display an abundance in several more-cytotoxic and late-differentiated peripheral immune subsets and elevated circulating levels of GZMA, while a reduction in regulatory or tolerance-inducing cell types. These various cellular and soluble factors synergistically form a systemic immune milieu that is more cytotoxic while being less regulatory.

Such an immune milieu might contribute to the pathogenesis of iPD. Those affected peripheral immune components represent prime candidates for novel easily-accessible immunotherapeutic options in order to control the progression of early-stage iPD.

Limitations of the Study

In this clinical study, no efforts have been put to investigate the underlying cellular and molecular mechanisms causing the more-cytotoxic and late-differentiated immune profile in early-to-mid PD, especially for iPD patients. We have previously described reduced T-cell immunoaging, i.e., 'younger' immune system, in both mice and patients with the deficiency of the key familial PD gene PARK7/DJ-1 via regulating the immunometabolic process (Danileviciute et al. 2022, Zeng et al. 2022). The accelerated differentiation in several immune subsets we observed in iPD patients might be also attributable to an immunometabolic dysregulation. Supporting this notion, mitochondrial deficiency has been indeed widely reported in both idiopathic and genetic PD (Abou-Sleiman et al. 2006, Bose and Beal 2016, Park et al. 2018).

It still remains unclear whether CD8 TEMRA in PD of our cohorts are specific against PD-relevant antigens or develop unspecifically due to the insufficient CD8 Treg control on the expansion or differentiation. A very recent study revealed that highly differentiated and expanded CD8 T cells share the same TCR clonotypes between the periphery and cerebrospinal fluid (CSF) of a small number of PD (Wang et al. 2021). However, the two types of samples have not been taken from the same individuals.

Materials & Methods

Cohort Design

We followed the ethical regulation of Luxembourg and obtained ethical approval from Luxembourg National Research Ethics Committee (CNER) (Hipp et al. 2018). Informed consent was obtained before each participant was recruited into the study by the local clinical team in Luxembourg. All study participants were recruited from the Luxembourg Parkinson's Study, a nation-wide, monocentric, observational longitudinal study with parallel healthy controls. The overall steps of selection are provided in **Figure 1**. As a first step, we screened for HC and iPD patients aged 60-70 years (except the 3 genetic patients: one PD patient with two rare variants, one pathogenic homozygote variant N409S in GBA and another non-pathogenic heterozygote rare variant in PINK1 A383T, aged 48 years; one PD case with non-pathogenic heterozygote variant K13R in GBA, aged 55 years; one PD patient with the homozygote pathogenic variant L369P in PINK1, aged 45 years). We narrowed the selection to early-to-mid stage PD having a mean disease duration of 6.6 years after diagnosis. Since aging is the primary risk factor for PD (Reeve et al. 2014) and aging

dramatically affects the immune system (Nikolich-Zugich 2018), we focused on a relatively narrow age window (60-70 years) in the PD and the corresponding HC group. We also excluded potential participants if they were diagnosed with any immune-associated diseases, such as diabetes, cancer, chronic inflammatory disease, autoimmune disease and acute infection or if they were currently treated with immunosuppressive medication (see **Table S1** for detailed overview of the exclusion criteria). After the first round of exclusion, 150 PD and 58 HC were further tested for their cytomegalovirus (CMV) serologic status based on biobanked serum samples. CMV has been well documented to facilitate the immunosenescence process (Jergovic et al. 2019). In order to make the immunological analysis comparable at such an advanced age, we only invited HC and PD subjects as participants for deep immune phenotyping analysis if they were seropositive for anti-CMV IgG. As a result, a total of 28 PD and 24 HC CMV positive individuals agreed to be included in this study requiring additional blood sampling (see **Table S2** for details on demographic and clinical information). To account for the circadian rhythm of immune cells trafficking throughout the body (Druzd et al. 2017), all blood samples of the participants were collected in the mornings and processed within six hours.

Detection of anti-CMV IgG

CMV infection is widely spread throughout the population and seropositivity correlates positively with age (Lachmann et al. 2018). Previous reports have shown that CMV infection promotes immune ageing (Jergovic et al. 2019). To exclude a potential bias in our analysis due to a differential CMV status in PD and HC, we measured the CMV serology of all the potential study participants (including HCs) fitting the inclusion and exclusion criteria and only selected participants who were seropositive for CMV (**Figure 1**). An ELISA was performed on plasma samples from previous visits that were preserved in the local biobank (Integrated Biobank of Luxembourg). We used the Human Anti-Cytomegalovirus IgG ELISA Kit (Abcam, ab108724) and followed manufacturer's instructions.

Mass cytometry (CyTOF) staining and analysis

Fresh whole blood was first incubated with Human TruStain FcX™ (FcX, 422302, Biolegend) for 10 min at room temperature (RT). Surface staining was performed by transfering the blood into the Maxpar® Direct Immune Profiling Assay (MDIPA, 201325, Fluidigm) tube containing a dry antibody pellet. To the antibody-blood mixture, we added four in-house-conjugated and two pre-conjugated antibodies (**Table S3**). To fit with our purpose, another four in-house-conjugated antibodies (C-Kit, KLRG1, NKP44 and CD49d) were labeled with Maxpar® X8 Antibody Labeling Kit (201142A, 201159A, 201162A or 201169A, Fluidigm). Incubation lasted for 30 min at RT. Immediately after staining was completed, Cal-lyse solution (GAS010, Thermo Fisher Scientific) was added to each tube for a 10-min incubation in the dark; then 3 mL of deionised water were added for another 10-

min incubation in the dark. Cells were washed twice with MaxPar Cell Staining Buffer (CSB, 201068, Fluidigm) (400 x g, RT, 10 min). Cells were then fixed with 1.6% of formaldehyde solution (Pierce 16% Formaldehyde, 289006, Thermo Fisher Scientific). Centrifugation conditions after fixation were 800 x g, for 10 min at 4°C. As a last step, samples were incubated with Ir-Intercalator (201192A, Fluidigm), diluted (1:2000) in MaxPar Fix&Perm (201067, Fluidigm), and rested at RT for 1 h. Then, the cells were stored at -80°C until the day of CyTOF acquisition. Prior to the acquisition, cells were washed twice with CSB and twice with Cell Acquisition Solution (CAS, 201239, Fluidigm). Cells were resuspended at 5E5 per mL in 1:10 calibration beads (EQ Four Element Calibration Beads, 201078, Fluidigm) diluted with CAS and the samples were analyzed with a HELIOS mass cytometer (Fluidigm) at a flow rate of 0.030 mL per min. Generated *.fcs files were normalized with the HELIOS acquisition software by using EQ beads as a standard. Of note, due to notable staining issues, we excluded CD25, CD16 and CD127 from the analysis. As a consequence, we were unable to gate and analyze Tregs in our CyTOF panel (**Fig. S1**). Alternatively, for non-classic monocyte and ILC gating, we used CD38 instead of CD16 as employed elsewhere (Picozza et al. 2013). For NK subset gating, we used CD56 and CD57 to distinguish immature, mature and terminally-differentiated NK subsets (Lopez-Vergès et al. 2010).

We mainly performed the supervised analysis based on manual gating (**Fig. S1**) while we also implemented an unsupervised analysis on gated CD8 T cells. The CD8+ T cells of 50 samples (23 HC, 27 PD; one HC sample was excluded due to a too low number of acquired cells; one PD sample was excluded due to the fact that a partially-wrong CyTOF staining panel was used) were extracted using FlowJo v10 to perform the viSNE analysis on the CellEngine (https://cellengine.com/). The viSNE analysis was achieved using all the cells from each fcs file, with 1000 iterations and a perplexity of 80. The following markers were used to generate the viSNE: CD45RA/CCR7/CD27/CD57/CD38/HLADR. Of note, except for the results presented in **Figure 2M**, all the other results were based on supervised analysis.

PBMC isolation

For detailed method description, please refer to our recent work. In brief, 10-ml vacutainer K2EDTA blood collection tubes (367525, BD) was used to sample blood from each participant in the morning. Peripheral blood mononuclear cells (PBMCs) were isolated from fresh whole blood by gradient centrifugation at 1200 x g for 20 min, RT using the SepMate™-50 tubes (85450, Stemcell) and Lymphoprep™ (07801, StemCell). The cells were washed three times with FCM (flow cytometry) buffer (Ca^{2+}/Mg^{2+} free PBS + 2% heat-inactivated FBS) and counted with a CASY cell counter.

Multi-panel multi-color flow cytometry analysis

Similar multi-panel multi-color (up to 18) FCM analysis has already been fully established and performed by us in other human-sample based studies(Capelle et al. 2022). To ease the comprehension, we described the major procedures here again. For each study participant, 1 million of fresh PBMCs were stained for each of the 5 staining panels. Prior to the cell staining, the PBMCs were incubated for 15 min at 4°C with 50 µL Brilliant Stain Buffer (BD, 563794), containing 2.5 µL Fc blocking antibodies (BD, 564765). 50 µL of 2 x concentrated surface antibody master mixes diluted in Brilliant Stain Buffer were added to the cell suspension and incubated for 30 min at 4°C (**Table S4**). Following three washing steps with FCM buffer (300 x g, 5 min, 4 °C), the stained PBMCs were fixed for 60 min at RT using the fixation reagent of the True-Nuclear Transcription Factor Buffer Set (Biolegend, 424401). After fixation, the cells were centrifuged (400 x g, 5 min, 4°C), re-suspended in 200 µL FCM buffer and left at 4°C overnight. The next day, the PBMCs were washed once in permeabilization buffer of the same kit and re-suspended in permeabilization buffer, containing 2.5 µL Fc blocking antibodies. After a 10-min incubation, the cells were centrifuged and the cell pellet was re-suspended in 100 µL permeabilization buffer containing the antibodies for the intracellular targets for a 30-40 min incubation at RT. Finally, the cells were washed three times in permeabilization buffer and re-suspended in 100 µL of FCM buffer for the acquisition on a BD LSRFortessa™. The data was analysed using the *FlowJo* v10 software. Of note, with our hypothesis-free approach, we could not foresee the CD8 TEMRA results. We never used CD45RA, CCR7 and CD27 in the same panel and this is why we had to demonstrate the CD8 TEMRA results by combining different gating strategies from different panels.

MSD assays to detect serological soluble factors

We used the MSD multiplex assay [U-PLEX Immuno-Oncology Group 1 (hu) Assay, K151AEL-1] to quantify the 10 selected serological soluable factors (Granzyme A, B, IFN-γ, IL-13, IL-33, IL-5, IL-8, GM-CSF, IP10 and MCP-1) following manufacture's recommendations in a procedure similar to that in our other clinical or human sample-based work(Capelle et al. 2022). For the MSD assay, the biobanked samples were undiluted. We used the perforin (PRF1) human ELISA kit (ab46068) purchased from Abcam to quantify serological perforin. For the peforin ELISA protocol, we first diluted all the serum samples 30 times, which was pre-determined by a test experiment. Of note, most of the serum samples were obtained at the same time as the fresh blood taken for flow cytometry analysis, while some of the sera were only available from the most recent visit (< one year).

Statistical analysis

Statistics analysis was performed in Graphpad Prism 9.0 using an unpaired two-tailed Student *t* test or the Mann-Whitney nonparametric unpaired test. ROC analysis, volcano plot and PCA analysis

were also performed using GraphPad Prism v9.0. The precise test method used for the different figures is also specified in the corresponding figure legends. The error bars in the related types of figures represent the standard deviation (s.d.). For a few participants, some of the clinical information was unavailable. In that case, the related analysis did not interpolate any values to replace those empty cells in the data tables.

Acknowledgements

We first would like to show our gratitude to all the participants of the Luxembourg Parkinson's Study cohort for their participation in this clinical research study. We thank the recruitment team and study nurses of Parkinson Research Clinic of CHL and the Clinical and Epidemiological Investigation Centre (CIEC) of LIH for their excellent support, especially Daniela Valoura Esteves for the coordination of the recruitment of healthy controls. We also highly appreciate the expert support of the processing and biorepository teams at the Integrated Biobank of Luxembourg (IBBL). This study was mainly supported by the Luxembourg Personalized Medicine Consortium (PMC) (CoPImmunoPD, PMC/2018/01, F.Q.H.). The study was also partially supported by Luxembourg National Research Fund (FNR) CORE programme grant (CORE/14/BM/8231540/GeDES, F.Q.H.), FNR AFR-RIKEN bilateral programme (TregBAR, 11228353, F.Q.H., R.B. and M.O.) and several PRIDE programme grants (PRIDE/11012546/NEXTIMMUNE, PRIDE/10907093/CRITICS and PRIDE/14254520/i2TRON, F.Q.H., R.K., M.O.) and an individual AFR grant (PDH-2015-1/9989160, N.Z. via the group of F.Q.H.). The Luxembourg Parkinson's study is funded within the National Centre of Excellence in Research on Parkinson's disease (NCER-PD) by FNR. The work of R.K. was further supported by an Excellence Grant in Research within the PEARL programme of the FNR. Some icons in Figure 1A were generated from BioRender.com.

Author contributions

C.M.C. contributed to the design of the study, performed the experiments, performed data analysis and drafted the manuscript. S.C., F.H., M.K., D.R., V.T., O.D., A.B. and N.Z. performed experiments. M.H., L.P. T.M. and R.K. participated in study design and coordinated the patient cohort recruitment and collection of the biological samples and clinical data. P.M. contributed to genetic PD confirmation and selection. A.C., R.B., R.K., and M.O. provided substantial insights and supervision to the project. M.O. and F.Q.H. conceived the project. F.Q.H oversaw the whole project and revised the manuscript together with M.O.

Conflict of Interest

The authors declare no conflict of interest.

Data Availability

All the raw fcs files of flow cytometry and mass cytometry datasets generated in this clinical study will be deposited into a leading cytometry repository (https://www.immport.org/home) upon acceptance.

References

Abou-Sleiman, P. M., Muqit, M. M. and Wood, N. W. (2006). "Expanding insights of mitochondrial dysfunction in Parkinson's disease." Nat Rev Neurosci **7**(3): 207-219.

Akimova, T., Beier, U. H., Wang, L., Levine, M. H. and Hancock, W. W. (2011). "Helios expression is a marker of T cell activation and proliferation." PLoS One **6**(8): e24226.

Bose, A. and Beal, M. F. (2016). "Mitochondrial dysfunction in Parkinson's disease." J Neurochem **139 Suppl 1**: 216-231.

Braak, H., Rub, U., Gai, W. P. and Del Tredici, K. (2003). "Idiopathic Parkinson's disease: possible routes by which vulnerable neuronal types may be subject to neuroinvasion by an unknown pathogen." J Neural Transm (Vienna) **110**(5): 517-536.

Capelle, C. M., Cire, S., Ammerlaan, W., Konstantinou, M., Balling, R., Betsou, F., Cosma, A., Ollert, M. and Hefeng, F. Q. (2021). "Standard Peripheral Blood Mononuclear Cell Cryopreservation Selectively Decreases Detection of Nine Clinically Relevant T Cell Markers." Immunohorizons **5**(8): 711-720.

Capelle, C. M., Ciré, S., Domingues, O., Ernens, I., Hedin, F., Fischer, A., Snoeck, C. J., Ammerlaan, W., Konstantinou, M., Grzyb, K., Skupin, A., Carty, C. L., Hilger, C., Gilson, G., Celebic, A., Wilmes, P., Del Sol, A., Kaplan, I. M., Betsou, F., Abdelrahman, T., Cosma, A., Vaillant, M., Fagherazzi, G., Ollert, M. and Hefeng, F. Q. (2022). "Combinatorial analysis reveals highly coordinated early-stage immune reactions that predict later antiviral immunity in mild COVID-19 patients." Cell Reports Medicine **3**(4): 100600.

Cayrol, C. and Girard, J. P. (2014). "IL-33: an alarmin cytokine with crucial roles in innate immunity, inflammation and allergy." Curr Opin Immunol **31**: 31-37.

Chou, J. P. and Effros, R. B. (2013). "T cell replicative senescence in human aging." Curr Pharm Des **19**(9): 1680-1698.

Churlaud, G., Pitoiset, F., Jebbawi, F., Lorenzon, R., Bellier, B., Rosenzwajg, M. and Klatzmann, D. (2015). "Human and Mouse CD8+CD25+FOXP3+ Regulatory T Cells at Steady State and during Interleukin-2 Therapy." Frontiers in Immunology **6**(171).

Correale, J. and Villa, A. (2010). "Role of CD8+ CD25+ Foxp3+ regulatory T cells in multiple sclerosis." Annals of Neurology **67**(5): 625-638.

Danileviciute, E., Zeng, N., Capelle, C. M., Paczia, N., Gillespie, M. A., Kurniawan, H., Benzarti, M., Merz, M. P., Coowar, D., Fritah, S., Vogt Weisenhorn, D. M., Gomez Giro, G., Grusdat, M., Baron, A., Guerin, C., Franchina, D. G., Leonard, C., Domingues, O., Delhalle, S., Wurst, W., Turner, J. D., Schwamborn, J. C., Meiser, J., Kruger, R., Ranish, J., Brenner, D., Linster, C. L., Balling, R., Ollert, M. and Hefeng, F. Q. (2022). "PARK7/DJ-1 promotes pyruvate dehydrogenase activity and maintains Treg homeostasis during ageing." Nat Metab **4**(5): 589-607.

Davis, M. M., Tato, C. M. and Furman, D. (2017). "Systems immunology: just getting started." Nat Immunol **18**(7): 725-732.

Deleidi, M., Jäggle, M. and Rubino, G. (2015). "Immune aging, dysmetabolism, and inflammation in neurological diseases." Frontiers in Neuroscience **9**.

Delhalle, S., Bode, S. F. N., Balling, R., Ollert, M. and He, F. Q. (2018). "A roadmap towards personalized immunology." NPJ Systems Biology and Applications **4**(1): 9.

Dorsey, E. R., Constantinescu, R., Thompson, J. P., Biglan, K. M., Holloway, R. G., Kieburtz, K., Marshall, F. J., Ravina, B. M., Schifitto, G., Siderowf, A. and Tanner, C. M. (2007). "Projected number of people with Parkinson disease in the most populous nations, 2005 through 2030." Neurology **68**(5): 384-386.

Druzd, D., Matveeva, O., Ince, L., Harrison, U., He, W., Schmal, C., Herzel, H., Tsang, A. H., Kawakami, N., Leliavski, A., Uhl, O., Yao, L., Sander, L. E., Chen, C. S., Kraus, K., de Juan, A., Hergenhan, S. M., Ehlers, M., Koletzko, B., Haas, R., Solbach, W., Oster, H. and Scheiermann, C. (2017). "Lymphocyte Circadian Clocks Control Lymph Node Trafficking and Adaptive Immune Responses." Immunity **46**(1): 120-132.

Emamzadeh, F. N. and Surguchov, A. (2018). "Parkinson's Disease: Biomarkers, Treatment, and Risk Factors." Front Neurosci **12**: 612.

675 Flippe, L., Bezie, S., Anegon, I. and Guillonneau, C. (2019). "Future prospects for CD8(+) regulatory T cells
676 in immune tolerance." Immunol Rev **292**(1): 209-224.

677 Fung, I. T. H., Sankar, P., Zhang, Y., Robison, L. S., Zhao, X., D'Souza, S. S., Salinero, A. E., Wang, Y.,
678 Qian, J., Kuentzel, M. L., Chittur, S. V., Temple, S., Zuloaga, K. L. and Yang, Q. (2020). "Activation of group
679 2 innate lymphoid cells alleviates aging-associated cognitive decline." J Exp Med **217**(4).

680 Galiano-Landeira, J., Torra, A., Vila, M. and Bove, J. (2020). "CD8 T cell nigral infiltration precedes
681 synucleinopathy in early stages of Parkinson's disease." Brain **143**(12): 3717-3733.

682 Galkina, E., Thatte, J., Dabak, V., Williams, M. B., Ley, K. and Braciale, T. J. (2005). "Preferential migration
683 of effector CD8+ T cells into the interstitium of the normal lung." J Clin Invest **115**(12): 3473-3483.

684 Gate, D., Saligrama, N., Leventhal, O., Yang, A. C., Unger, M. S., Middeldorp, J., Chen, K., Lehallier, B.,
685 Channappa, D., De Los Santos, M. B., McBride, A., Pluvinage, J., Elahi, F., Tam, G. K., Kim, Y., Greicius,
686 M., Wagner, A. D., Aigner, L., Galasko, D. R., Davis, M. M. and Wyss-Coray, T. (2020). "Clonally expanded
687 CD8 T cells patrol the cerebrospinal fluid in Alzheimer's disease." Nature **577**(7790): 399-404.

688 Golebski, K., Layhadi, J. A., Sahiner, U., Steveling-Klein, E. H., Lenormand, M. M., Li, R. C. Y., Bal, S. M.,
689 Heesters, B. A., Vilà-Nadal, G., Hunewald, O., Montamat, G., He, F. Q., Ollert, M., Fedina, O., Lao-Araya,
690 M., Vijverberg, S. J. H., Maitland-van der Zee, A.-H., van Drunen, C. M., Fokkens, W. J., Durham, S. R.,
691 Spits, H. and Shamji, M. H. (2021). "Induction of IL-10-producing type 2 innate lymphoid cells by allergen
692 immunotherapy is associated with clinical response." Immunity **54**(2): 291-307.e297.

693 Goronzy, J. J. and Weyand, C. M. (2013). "Understanding immunosenescence to improve responses to
694 vaccines." Nature Immunology **14**(5): 428-436.

695 Goronzy, J. J. and Weyand, C. M. (2017). "Successful and Maladaptive T Cell Aging." Immunity **46**(3): 364-
696 378.

697 He, F. and Balling, R. (2013). "The role of regulatory T cells in neurodegenerative diseases." Wiley
698 Interdiscip Rev Syst Biol Med **5**(2): 153-180.

699 Hiam-Galvez, K. J., Allen, B. M. and Spitzer, M. H. (2021). "Systemic immunity in cancer." Nature Reviews
700 Cancer **21**(6): 345-359.

701 Hipp, G., Vaillant, M., Diederich, N. J., Roomp, K., Satagopam, V. P., Banda, P., Sandt, E., Mommaerts, K.,
702 Schmitz, S. K., Longhino, L., Schweicher, A., Hanff, A. M., Nicolai, B., Kolber, P., Reiter, D., Pavelka, L.,
703 Binck, S., Pauly, C., Geffers, L., Betsou, F., Gantenbein, M., Klucken, J., Gasser, T., Hu, M. T., Balling, R.
704 and Kruger, R. (2018). "The Luxembourg Parkinson's Study: A Comprehensive Approach for Stratification
705 and Early Diagnosis." Front Aging Neurosci **10**: 326.

706 Hoyler, T., Klose, C. S., Souabni, A., Turqueti-Neves, A., Pfeifer, D., Rawlins, E. L., Voehringer, D.,
707 Busslinger, M. and Diefenbach, A. (2012). "The transcription factor GATA-3 controls cell fate and
708 maintenance of type 2 innate lymphoid cells." Immunity **37**(4): 634-648.

709 Intlekofer, A. M., Takemoto, N., Wherry, E. J., Longworth, S. A., Northrup, J. T., Palanivel, V. R., Mullen, A.
710 C., Gasink, C. R., Kaech, S. M., Miller, J. D., Gapin, L., Ryan, K., Russ, A. P., Lindsten, T., Orange, J. S.,
711 Goldrath, A. W., Ahmed, R. and Reiner, S. L. (2005). "Effector and memory CD8+ T cell fate coupled by T-
712 bet and eomesodermin." Nat Immunol **6**(12): 1236-1244.

713 Inzelberg, R. and Jankovic, J. (2007). "Are Parkinson disease patients protected from some but not all
714 cancers?" Neurology **69**(15): 1542-1550.

715 Jergovic, M., Contreras, N. A. and Nikolich-Zugich, J. (2019). "Impact of CMV upon immune aging: facts and
716 fiction." Med Microbiol Immunol **208**(3-4): 263-269.

717 Jiang, S., Gao, H., Luo, Q., Wang, P. and Yang, X. (2017). "The correlation of lymphocyte subsets, natural
718 killer cell, and Parkinson's disease: a meta-analysis." Neurol Sci **38**(8): 1373-1380.

719 Josefowicz, S. Z., Lu, L.-F. and Rudensky, A. Y. (2012). "Regulatory T Cells: Mechanisms of Differentiation
720 and Function." Annual Review of Immunology **30**(1): 531-564.

721 Kaech, S. M., Tan, J. T., Wherry, E. J., Konieczny, B. T., Surh, C. D. and Ahmed, R. (2003). "Selective
722 expression of the interleukin 7 receptor identifies effector CD8 T cells that give rise to long-lived memory
723 cells." Nature Immunology **4**(12): 1191-1198.

Kiniwa, Y., Miyahara, Y., Wang, H. Y., Peng, W., Peng, G., Wheeler, T. M., Thompson, T. C., Old, L. J. and Wang, R.-F. (2007). "CD8⁺ Foxp3⁺ Regulatory T Cells Mediate Immunosuppression in Prostate Cancer." Clinical Cancer Research **13**(23): 6947-6958.

Knox, J. J., Cosma, G. L., Betts, M. R. and McLane, L. M. (2014). "Characterization of T-Bet and Eomes in Peripheral Human Immune Cells." Frontiers in Immunology **5**.

Koch, S., Labri, A., Özelik, D., Solana, R., Gouttefangeas, C., Attig, S., Wikby, A., Strindhal, J., Franceschi, C. and Pawlec, G. (2007). "Cytomegalovirus Infection." Annals of the New York Academy of Sciences **1114**(1): 23-35.

Kustrimovic, N., Comi, C., Magistrelli, L., Rasini, E., Legnaro, M., Bombelli, R., Aleksic, I., Blandini, F., Minafra, B., Riboldazzi, G., Sturchio, A., Mauri, M., Bono, G., Marino, F. and Cosentino, M. (2018). "Parkinson's disease patients have a complex phenotypic and functional Th1 bias: cross-sectional studies of CD4+ Th1/Th2/T17 and Treg in drug-naive and drug-treated patients." J Neuroinflammation **15**(1): 205.

Lachmann, R., Loenenbach, A., Waterboer, T., Brenner, N., Pawlita, M., Michel, A., Thamm, M., Poethko-Muller, C., Wichmann, O. and Wiese-Posselt, M. (2018). "Cytomegalovirus (CMV) seroprevalence in the adult population of Germany." PLoS One **13**(7): e0200267.

Lee, K. A., Shin, K. S., Kim, G. Y., Song, Y. C., Bae, E. A., Kim, I. K., Koh, C. H. and Kang, C. Y. (2016). "Characterization of age-associated exhausted CD8(+) T cells defined by increased expression of Tim-3 and PD-1." Aging Cell **15**(2): 291-300.

Li, S., Xie, Q., Zeng, Y., Zou, C., Liu, X., Wu, S., Deng, H., Xu, Y., Li, X. C. and Dai, Z. (2014). "A naturally occurring CD8+CD122+ T-cell subset as a memory-like Treg family." Cellular & Molecular Immunology **11**(4): 326-331.

Lindestam Arlehamn, C. S., Dhanwani, R., Pham, J., Kuan, R., Frazier, A., Rezende Dutra, J., Phillips, E., Mallal, S., Roederer, M., Marder, K. S., Amara, A. W., Standaert, D. G., Goldman, J. G., Litvan, I., Peters, B., Sulzer, D. and Sette, A. (2020). "alpha-Synuclein-specific T cell reactivity is associated with preclinical and early Parkinson's disease." Nat Commun **11**(1): 1875.

Liu, J., Hill, B. J., Darko, S., Song, K., Quigley, M. F., Asher, T. E., Morita, Y., Greenaway, H. Y., Venturi, V., Douek, D. C., Davenport, M. P., Price, D. A. and Roederer, M. (2019). "The peripheral differentiation of human natural killer T cells." Immunol Cell Biol **97**(6): 586-596.

Lopez-Vergès, S., Milush, J. M., Pandey, S., York, V. A., Arakawa-Hoyt, J., Pircher, H., Norris, P. J., Nixon, D. F. and Lanier, L. L. (2010). "CD57 defines a functionally distinct population of mature NK cells in the human CD56dimCD16+ NK-cell subset." Blood **116**(19): 3865-3874.

Louveau, A., Harris, T. H. and Kipnis, J. (2015). "Revisiting the Mechanisms of CNS Immune Privilege." Trends Immunol **36**(10): 569-577.

Mandrekar, J. N. (2010). "Receiver Operating Characteristic Curve in Diagnostic Test Assessment." Journal of Thoracic Oncology **5**(9): 1315-1316.

Matheoud, D., Cannon, T., Voisin, A., Penttinen, A. M., Ramet, L., Fahmy, A. M., Ducrot, C., Laplante, A., Bourque, M. J., Zhu, L., Cayrol, R., Le Campion, A., McBride, H. M., Gruenheid, S., Trudeau, L. E. and Desjardins, M. (2019). "Intestinal infection triggers Parkinson's disease-like symptoms in Pink1(-/-) mice." Nature **571**(7766): 565-569.

Metkar, S. S., Menaa, C., Pardo, J., Wang, B., Wallich, R., Freudenberg, M., Kim, S., Raja, S. M., Shi, L., Simon, M. M. and Froelich, C. J. (2008). "Human and Mouse Granzyme A Induce a Proinflammatory Cytokine Response." Immunity **29**(5): 720-733.

Moro, K., Yamada, T., Tanabe, M., Takeuchi, T., Ikawa, T., Kawamoto, H., Furusawa, J.-i., Ohtani, M., Fujii, H. and Koyasu, S. (2010). "Innate production of TH2 cytokines by adipose tissue-associated c-Kit+Sca-1+ lymphoid cells." Nature **463**(7280): 540-544.

Munoz-Delgado, L., Macias-Garcia, D., Jesus, S., Martin-Rodriguez, J. F., Labrador-Espinosa, M. A., Jimenez-Jaraba, M. V., Adarmes-Gomez, A., Carrillo, F. and Mir, P. (2021). "Peripheral Immune Profile and Neutrophil-to-Lymphocyte Ratio in Parkinson's Disease." Mov Disord.

Nikolich-Zugich, J. (2018). "The twilight of immunity: emerging concepts in aging of the immune system." Nat Immunol **19**(1): 10-19.

Nussbaum, J. C., Van Dyken, S. J., von Moltke, J., Cheng, L. E., Mohapatra, A., Molofsky, A. B., Thornton, E. E., Krummel, M. F., Chawla, A., Liang, H. E. and Locksley, R. M. (2013). "Type 2 innate lymphoid cells control eosinophil homeostasis." Nature **502**(7470): 245-248.

Park, J. S., Davis, R. L. and Sue, C. M. (2018). "Mitochondrial Dysfunction in Parkinson's Disease: New Mechanistic Insights and Therapeutic Perspectives." Curr Neurol Neurosci Rep **18**(5): 21.

Parnetti, L., Gaetani, L., Eusebi, P., Paciotti, S., Hansson, O., El-Agnaf, O., Mollenhauer, B., Blennow, K. and Calabresi, P. (2019). "CSF and blood biomarkers for Parkinson's disease." Lancet Neurol **18**(6): 573-586.

Pereira, B. I. and Akbar, A. N. (2016). "Convergence of Innate and Adaptive Immunity during Human Aging." Frontiers in Immunology **7**(445).

Picozza, M., Battistini, L. and Borsellino, G. (2013). "Mononuclear phagocytes and marker modulation: when CD16 disappears, CD38 takes the stage." Blood **122**(3): 456-457.

Poewe, W., Seppi, K., Tanner, C. M., Halliday, G. M., Brundin, P., Volkmann, J., Schrag, A. E. and Lang, A. E. (2017). "Parkinson disease." Nat Rev Dis Primers **3**: 17013.

Popescu, I., Pipeling, M. R., Shah, P. D., Orens, J. B. and McDyer, J. F. (2014). "T-bet:Eomes balance, effector function, and proliferation of cytomegalovirus-specific CD8+ T cells during primary infection differentiates the capacity for durable immune control." J Immunol **193**(11): 5709-5722.

Qin, X. Y., Zhang, S. P., Cao, C., Loh, Y. P. and Cheng, Y. (2016). "Aberrations in Peripheral Inflammatory Cytokine Levels in Parkinson Disease: A Systematic Review and Meta-analysis." JAMA Neurol **73**(11): 1316-1324.

Reale, M., Iarlori, C., Thomas, A., Gambi, D., Perfetti, B., Di Nicola, M. and Onofrj, M. (2009). "Peripheral cytokines profile in Parkinson's disease." Brain Behav Immun **23**(1): 55-63.

Reeve, A., Simcox, E. and Turnbull, D. (2014). "Ageing and Parkinson's disease: why is advancing age the biggest risk factor?" Ageing Res Rev **14**: 19-30.

Russi, A. E., Walker-Caulfield, M. E., Ebel, M. E. and Brown, M. A. (2015). "Cutting edge: c-Kit signaling differentially regulates type 2 innate lymphoid cell accumulation and susceptibility to central nervous system demyelination in male and female SJL mice." J Immunol **194**(12): 5609-5613.

Sakaguchi, S., Yamaguchi, T., Nomura, T. and Ono, M. (2008). "Regulatory T cells and immune tolerance." Cell **133**(5): 775-787.

Sasaki, K., Zhu, X., Vasquez, C., Nishimura, F., Dusak, J. E., Huang, J., Fujita, M., Wesa, A., Potter, D. M., Walker, P. R., Storkus, W. J. and Okada, H. (2007). "Preferential Expression of Very Late Antigen-4 on Type 1 CTL Cells Plays a Critical Role in Trafficking into Central Nervous System Tumors." Cancer Research **67**(13): 6451-6458.

Saunders, J. A., Estes, K. A., Kosloski, L. M., Allen, H. E., Dempsey, K. M., Torres-Russotto, D. R., Meza, J. L., Santamaria, P. M., Bertoni, J. M., Murman, D. L., Ali, H. H., Standaert, D. G., Mosley, R. L. and Gendelman, H. E. (2012). "CD4+ regulatory and effector/memory T cell subsets profile motor dysfunction in Parkinson's disease." J Neuroimmune Pharmacol **7**(4): 927-938.

Schmidt, A., Oberle, N. and Krammer, P. (2012). "Molecular Mechanisms of Treg-Mediated T Cell Suppression." Frontiers in Immunology **3**(51).

Shutinoski, B., Hakimi, M., Harmsen, I. E., Lunn, M., Rocha, J., Lengacher, N., Zhou, Y. Y., Khan, J., Nguyen, A., Hake-Volling, Q., El-Kodsi, D., Li, J., Alikashani, A., Beauchamp, C., Majithia, J., Coombs, K., Shimshek, D., Marcogliese, P. C., Park, D. S., Rioux, J. D., Philpott, D. J., Woulfe, J. M., Hayley, S., Sad, S., Tomlinson, J. J., Brown, E. G. and Schlossmacher, M. G. (2019). "Lrrk2 alleles modulate inflammation during microbial infection of mice in a sex-dependent manner." Science Translational Medicine **11**(511): eaas9292.

Sommer, A., Marxreiter, F., Krach, F., Fadler, T., Grosch, J., Maroni, M., Graef, D., Eberhardt, E., Riemenschneider, M. J., Yeo, G. W., Kohl, Z., Xiang, W., Gage, F. H., Winkler, J., Prots, I. and Winner, B. (2018). "Th17 Lymphocytes Induce Neuronal Cell Death in a Human iPSC-Based Model of Parkinson's Disease." Cell Stem Cell **23**(1): 123-131 e126.

Spits, H. and Di Santo, J. P. (2011). "The expanding family of innate lymphoid cells: regulators and effectors of immunity and tissue remodeling." Nat Immunol **12**(1): 21-27.

Storelli, E., Cassina, N., Rasini, E., Marino, F. and Cosentino, M. (2019). "Do Th17 Lymphocytes and IL-17 Contribute to Parkinson's Disease? A Systematic Review of Available Evidence." Front Neurol **10**: 13.

Strioga, M., Pasukoniene, V. and Characiejus, D. (2011). "CD8+ CD28- and CD8+ CD57+ T cells and their role in health and disease." Immunology **134**(1): 17-32.

Sullivan, B. M., Juedes, A., Szabo, S. J., von Herrath, M. and Glimcher, L. H. (2003). "Antigen-driven effector CD8 T cell function regulated by T-bet." Proc Natl Acad Sci U S A **100**(26): 15818-15823.

Sulzer, D., Alcalay, R. N., Garretti, F., Cote, L., Kanter, E., Agin-Liebes, J., Liong, C., McMurtrey, C., Hildebrand, W. H., Mao, X., Dawson, V. L., Dawson, T. M., Oseroff, C., Pham, J., Sidney, J., Dillon, M. B., Carpenter, C., Weiskopf, D., Phillips, E., Mallal, S., Peters, B., Frazier, A., Lindestam Arlehamn, C. S. and Sette, A. (2017). "T cells from patients with Parkinson's disease recognize alpha-synuclein peptides." Nature **546**(7660): 656-661.

Thome, A. D., Atassi, F., Wang, J., Faridar, A., Zhao, W., Thonhoff, J. R., Beers, D. R., Lai, E. C. and Appel, S. H. (2021). "Ex vivo expansion of dysfunctional regulatory T lymphocytes restores suppressive function in Parkinson's disease." NPJ Parkinsons Dis **7**(1): 41.

van Daalen, K. R., Reijneveld, J. F. and Bovenschen, N. (2020). "Modulation of Inflammation by Extracellular Granzyme A." Frontiers in Immunology **11**.

Wang, P., Yao, L., Luo, M., Zhou, W., Jin, X., Xu, Z., Yan, S., Li, Y., Xu, C., Cheng, R., Huang, Y., Lin, X., Ma, K., Cao, H., Liu, H., Xue, G., Han, F., Nie, H. and Jiang, Q. (2021). "Single-cell transcriptome and TCR profiling reveal activated and expanded T cell populations in Parkinson's disease." Cell Discov **7**(1): 52.

Wang, Q., Liu, Y. and Zhou, J. (2015). "Neuroinflammation in Parkinson's disease and its potential as therapeutic target." Transl Neurodegener **4**: 19.

Wang, Y., Gao, H., Jiang, S., Luo, Q., Han, X., Xiong, Y., Xu, Z., Qiao, R. and Yang, X. (2021). "Principal component analysis of routine blood test results with Parkinson's disease: A case-control study." Exp Gerontol **144**: 111188.

Weng, N. P. (2006). "Aging of the immune system: how much can the adaptive immune system adapt?" Immunity **24**(5): 495-499.

Wherry, E. J. (2011). "T cell exhaustion." Nat Immunol **12**(6): 492-499.

Williams-Gray, C. H., Wijeyekoon, R. S., Scott, K. M., Hayat, S., Barker, R. A. and Jones, J. L. (2018). "Abnormalities of age-related T cell senescence in Parkinson's disease." J Neuroinflammation **15**(1): 166.

Woodland, D. L. and Kohlmeier, J. E. (2009). "Migration, maintenance and recall of memory T cells in peripheral tissues." Nat Rev Immunol **9**(3): 153-161.

Yednock, T. A., Cannon, C., Fritz, L. C., Sanchez-Madrid, F., Steinman, L. and Karin, N. (1992). "Prevention of experimental autoimmune encephalomyelitis by antibodies against α4βI integrin." Nature **356**(6364): 63-66.

Yi, J. S., Cox, M. A. and Zajac, A. J. (2010). "T-cell exhaustion: characteristics, causes and conversion." Immunology **129**(4): 474-481.

Zeng, H., Yang, K., Cloer, C., Neale, G., Vogel, P. and Chi, H. (2013). "mTORC1 couples immune signals and metabolic programming to establish T(reg)-cell function." Nature **499**(7459): 485-490.

Zeng, N., Capelle, C. M., Baron, A., Kobayashi, T., Cire, S., Tslaf, V., Leonard, C., Coowar, D., Koseki, H., Westendorf, A. M., Buer, J., Brenner, D., Kruger, R., Balling, R., Ollert, M. and Hefeng, F. Q. (2022). "DJ-1 depletion prevents immunoaging in T-cell compartments." EMBO Rep **23**(3): e53302.

Zhang, S., Wu, M. and Wang, F. (2018). "Immune regulation by CD8(+) Treg cells: novel possibilities for anticancer immunotherapy." Cell Mol Immunol **15**(9): 805-807.

Main Figures and Legends

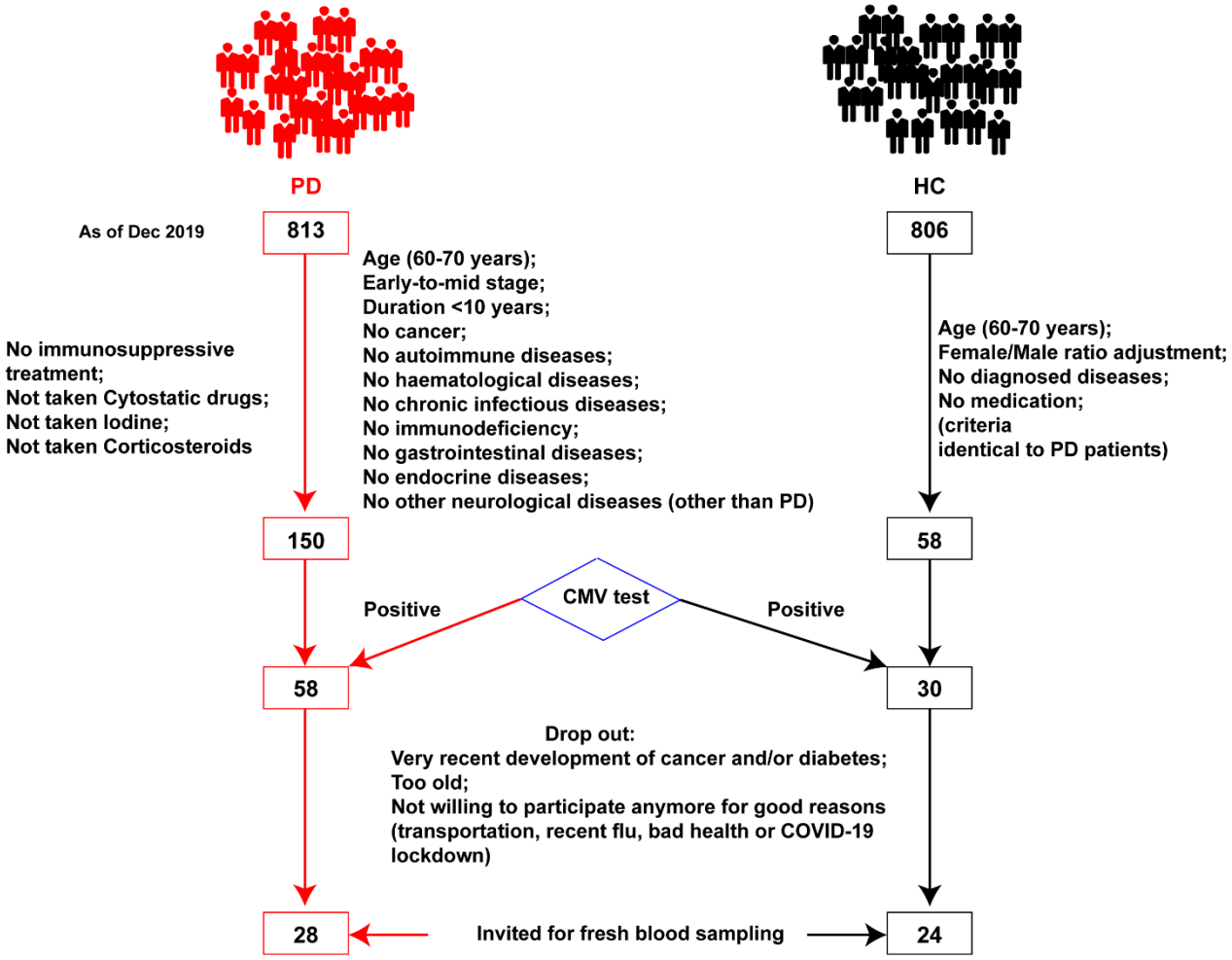

873
874

875 **Figure 1. Cohort design for fresh-blood-based deep immunophenotyping analysis.**

876 Schematic representation showing the selection of the participants from the ongoing nation-wide
877 Luxembourg Parkinson's Study in this work. The comorbidities indicate that PD or HC have never
878 been diagnosed with any of those diseases. For the medications, it refers to the scenario that there
879 were no record in receiving those treatments of the given participant. For the the limit of disease
880 duration (<10 years), we exceptionally included three participants with longer duration (refer to
881 **Material and Methods**). HC, healthy controls; PD, patients with Parkinson's disease; CMV,
882 cytomegalovirus.

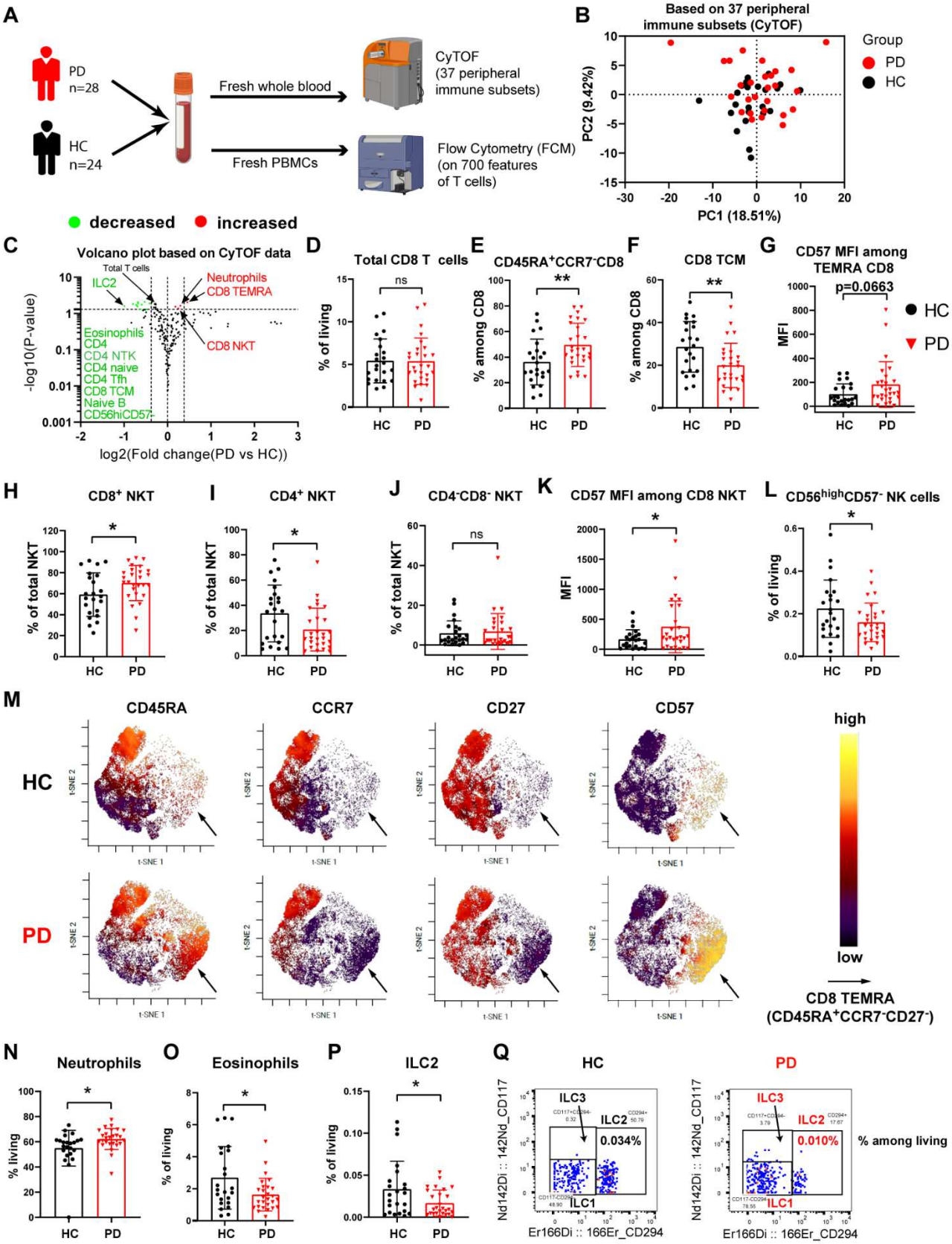
A
PD
n=28
HC
n=24
Fresh whole blood
Fresh PBMCs
CyTOF
(37 peripheral
immune subsets)
Flow Cytometry (FCM)
(on 700 features
of T cells)
B
Based on 37 peripheral
immune subsets (CyTOF)
Group
PD
HC
PC2 (9.42%)
PC1 (18.51%)
decreased
increased
C
Volcano plot based on CyTOF data
Total T cells
ILC2
Neutrophils
CD8 TEMRA
CD8 NKT
Eosinophils
CD4
CD4 NTK
CD4 naive
CD4 Tfh
CD8 TCM
Naive B
CD56hiCD57-
-log10(P-value)
log2(Fold change(PD vs HC))
D
Total CD8 T cells
ns
% of living
E
CD45RA+CCR7-CD8
**
% among CD8
F
CD8 TCM
**
% among CD8
G
CD57 MFI among
TEMRA CD8
p=0.0663
MFI
HC
PD
H
CD8+ NKT
*
% of total NKT
I
CD4+ NKT
*
% of total NKT
J
CD4-CD8- NKT
ns
% of total NKT
K
CD57 MFI among CD8 NKT
*
MFI
L
CD56highCD57- NK cells
*
% of living
M
CD45RA
CCR7
CD27
CD57
HC
PD
t-SNE 1
t-SNE 2
high
low
CD8 TEMRA
(CD45RA+CCR7-CD27-)
N
Neutrophils
*
% living
O
Eosinophils
*
% of living
P
ILC2
*
% of living
Q
HC
PD
ILC3
ILC2
ILC1
0.034%
0.010%
% among living
Nd142Di :: 142Nd_CD117
Er166Di :: 166Er_CD294

Figure 2. Single-cell CyTOF analysis shows a more-cytotoxic and late-differentiated immune profile in early-to-mid iPD.

(**A**) Graphical representation describing the cohort and the experimental setup. (**B**) PCA plot showing no distinct immunological fingerprint based on the entire peripheral immune system analysed by CyTOF. (**C**) Volcano plot showing the most significantly ($p<0.05$, fold change >1.3) decreased (green) and increased (red) immune cell populations in PD compared to HC. The dashed line in the y axis corresponds to the value of 1.3 ($p=0.05$), while the two dashed lines in the x axis correspond to the value of -0.3785 or 0.3785 (a change fold of 1.3). (**D-G**) Scatter dot plots showing the frequency of total CD8 T cells among living $CD45^+$ singlets (**D**), CD8 $CD45RA^+CCR7^-$ (the simplified gating strategy for TEMRA) (**E**), CD8 TCM (central memory) (**F**) and CD57 geometric mean (MFI, **G**) among CD8 TEMRA. (**H-L**) Scatter dot plots showing the frequency of $CD8^+$ NKT (**H**), $CD4^+$ NKT cells (**I**) and CD4/CD8 double negative (DN) NKT (**J**) and CD57 geometric mean (MFI) (**K**) among total NKT. (**L**), the frequency of $CD56^{hi}CD57^-$ immature NK cells among living CD45+ cells. (**M**) Representative viSNE plot of one donor from either HC (upper panel) or PD (lower panel) highlighting the expression levels of CD45RA, CCR7, CD27 and CD57 in total CD8 T cells. The arrow indicates the CD8 $CD45RA^+CCR7^-CD27^-$ (TEMRA). (**N**-**P**) Scatter dot plots showing the frequency of innate lymphoid cell type 2 (ILC2, **N**), neutrophils (**O**) and eosinophils (**P**) among living $CD45^+$ immune cells. (**Q**) Representative cytometry plots showing the reduced frequency of ILC2 in PD. The enlarged number (rather than the small number in the original plot showing the frequency in the parent gate) showing the frequency among total living $CD45^+$ cells (refer to **Figure S1**). The results in (**D-L. N-P**) were analysed using an unpaired two-tailed Student *t* test. Data are presented as mean ± standard deviation (s.d.). Each symbol represents the measurement from one individual participant (**D-L, N-P**). As we explained in the text, the frequency among total living $CD45^+$ singlets reflected the number of cells for the given immune subset. ns or unlabelled, not significant; *p<=0.05, **p<=0.01, and ***p<=0.001. CyTOF, mass cytometry; CMV, cytomegalovirus; PBMC, peripheral blood mononuclear cells; HC, healthy controls; PD, patients with Parkinson's disease.

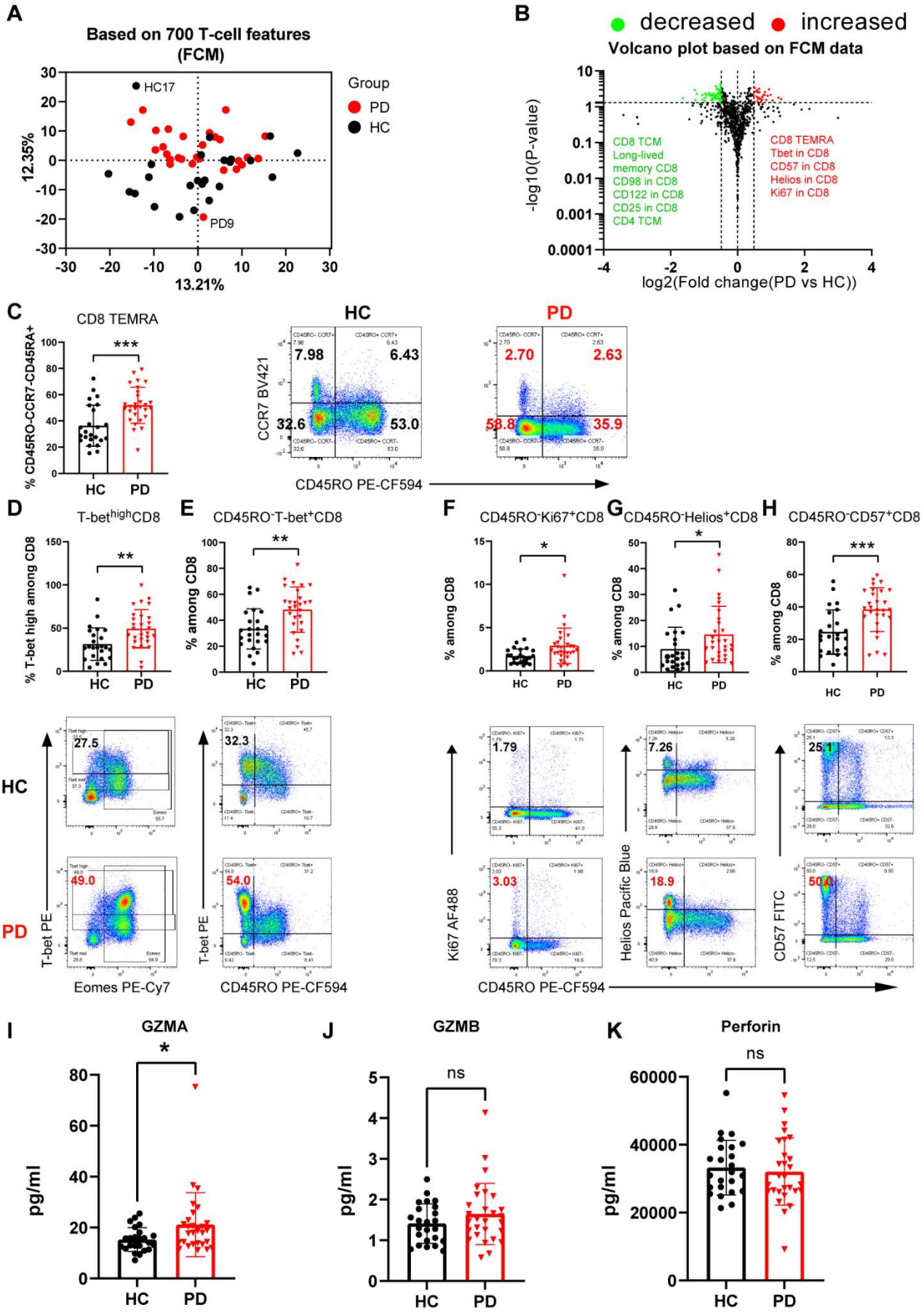
A
Based on 700 T-cell features (FCM)
HC17
PD9
Group
PD
HC
12.35%
13.21%
B
decreased
increased
Volcano plot based on FCM data
-log10(P-value)
log2(Fold change(PD vs HC))
CD8 TCM
Long-lived memory CD8
CD98 in CD8
CD122 in CD8
CD25 in CD8
CD4 TCM
CD8 TEMRA
Tbet in CD8
CD57 in CD8
Helios in CD8
Ki67 in CD8
C
CD8 TEMRA
% CD45RO-CCR7-CD45RA+
HC
PD
CCR7 BV421
CD45RO PE-CF594
7.98
6.43
32.6
53.0
2.70
2.63
58.8
35.9
D
T-bet^high CD8
% T-bet high among CD8
E
CD45RO-T-bet+CD8
% among CD8
F
CD45RO-Ki67+CD8
G
CD45RO-Helios+CD8
H
CD45RO-CD57+CD8
27.5
32.3
49.0
54.0
T-bet PE
Eomes PE-Cy7
CD45RO PE-CF594
1.79
7.26
25.1
3.03
18.9
50.4
Ki67 AF488
Helios Pacific Blue
CD57 FITC
I
GZMA
pg/ml
J
GZMB
K
Perforin
ns

911

Figure 3. Early-to-mid iPD exhibit an increased effector profile in CD8 T cells.

(**A**) PCA plot showing a distinct immunological fingerprint based on T-cell combinatorial features using flow-cytometry (FCM) analysis. (**B**) Volcano plot showing the most significantly ($p<0.05$, fold change >1.4) decreased (green) and increased (red) - cell subpopulations in PD compared to HCs. TCM, central memory. The dashed line in the y axis corresponds to the value of 1.3 ($p=0.05$), while the two dashed lines in x axis correspond to the value of -0.485 or 0.485 (a change fold of 1.4). (**C**) Scatter dot plots (left) and representative flow cytometry plots (right) showing the increase in CD8 TEMRA ($CD45O^{-}CD45RA^{+}CCR7^{-}$, the simplified gating strategy for TEMRA without considering CD27) in PD. The combination of markers used to define TEMRA was described in the title of y axis. (**D-H**) Scatter dot plots (upper panel) and representative flow-cytometry plots (lower panel) showing the frequency of $T\text{-}bet^{high}$ (**D**), $CD45RO^{-}T\text{-}bet^{+}$ (**E**), $CD45RO^{-}Ki67^{+}$ (**F**), $CD45RO^{-}Helios^{+}$ CD8 T cells (**G**) and CD45RO-CD57+ (**H**) in PD and HC. (**I-K**) The serological levels of GZMA (**I**), GZMB (**J**) and perforin (**K**). The results in **C-H** were analysed using an unpaired two-tailed Student *t* test while the results in **I-K** were analysed using the Mann-Whitney nonparametric unpaired test. Data are presented as mean ± standard deviation (s.d.). Each symbol represents the measurement from one individual participant (**C-K**). ns or unlabelled, not significant; *p<=0.05, **p<=0.01, and ***p<=0.001. HC, healthy controls; PD, patients with Parkinson's disease; FCM, flow cytometry.

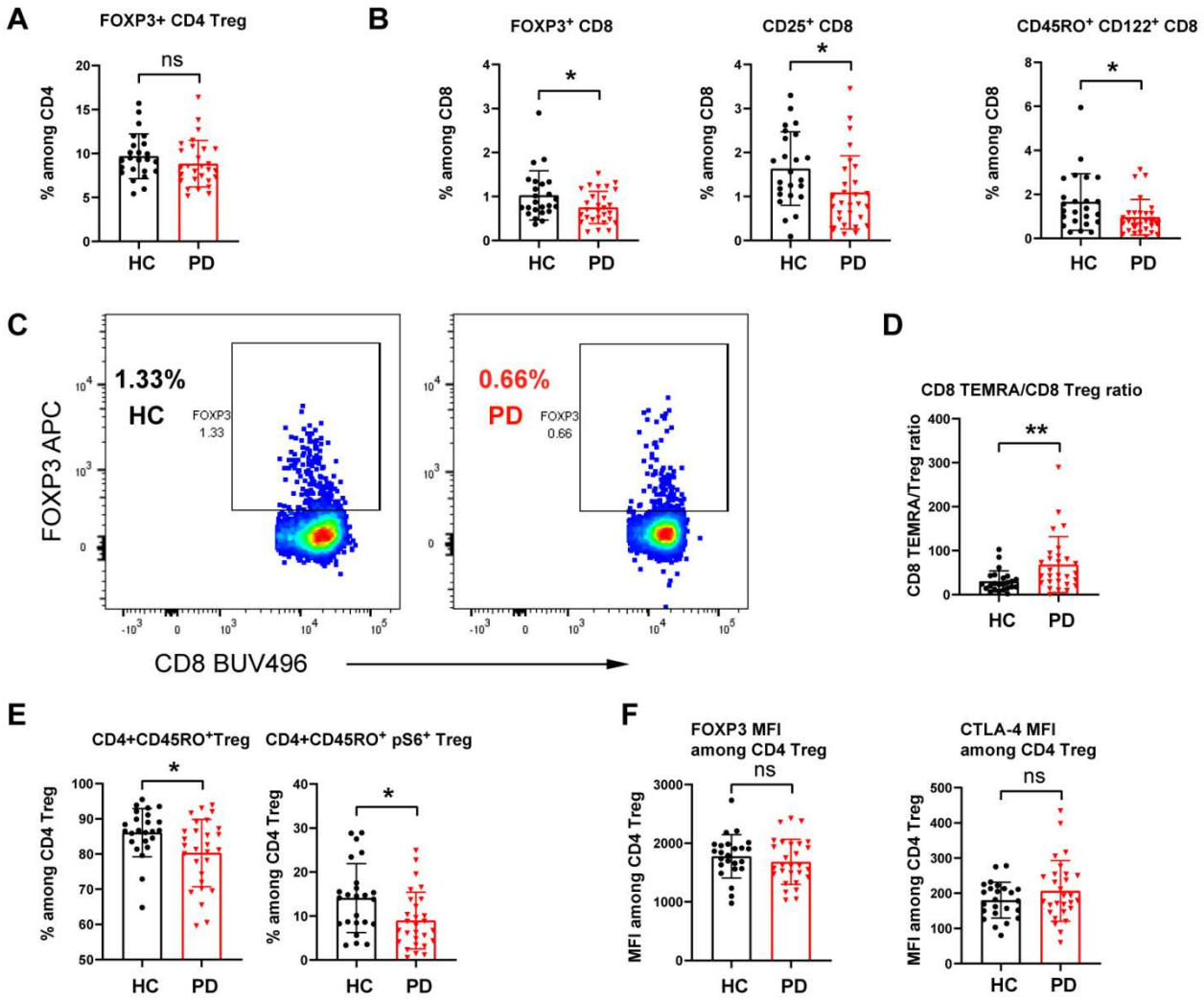

Figure 4. Early-to-mid iPD display a frequency reduction of CD8 Treg but not CD4 Treg.

(**A**) Scatter dot plot showing the frequency of FOXP3+ cells among CD4 T cells. (**B**) Scatter dot plots showing the frequency of FOXP3+, CD25+ and CD122+ among CD8 T cells. (**C**) Representative flow-cytometry plots showing the reduced frequency of FOXP3+ CD8 T cells. (**D**) Scatter dot plots showing the ratio between CD8 TEMRA and CD8 Treg. (**E**) Scatter dot plots showing the frequency of CD45RO+ and CD45RO+pS6+ among CD4 Treg in PD and HC. (**F**) Scatter dot plots showing the geometric mean (geomean, known as MFI) of FOXP3 and CTLA4 among total CD4+FOXP3+ Treg. The results were analysed using an unpaired two-tailed Student *t* test. Data are presented as mean ± standard deviation (s.d.). Each symbol represents the measurement from one individual participant (**A,B, D-F**). ns or unlabelled, not significant; *p<=0.05,

942 **p<=0.01, and ***p<=0.001. HC, healthy controls; PD, patients with Parkinson's disease.

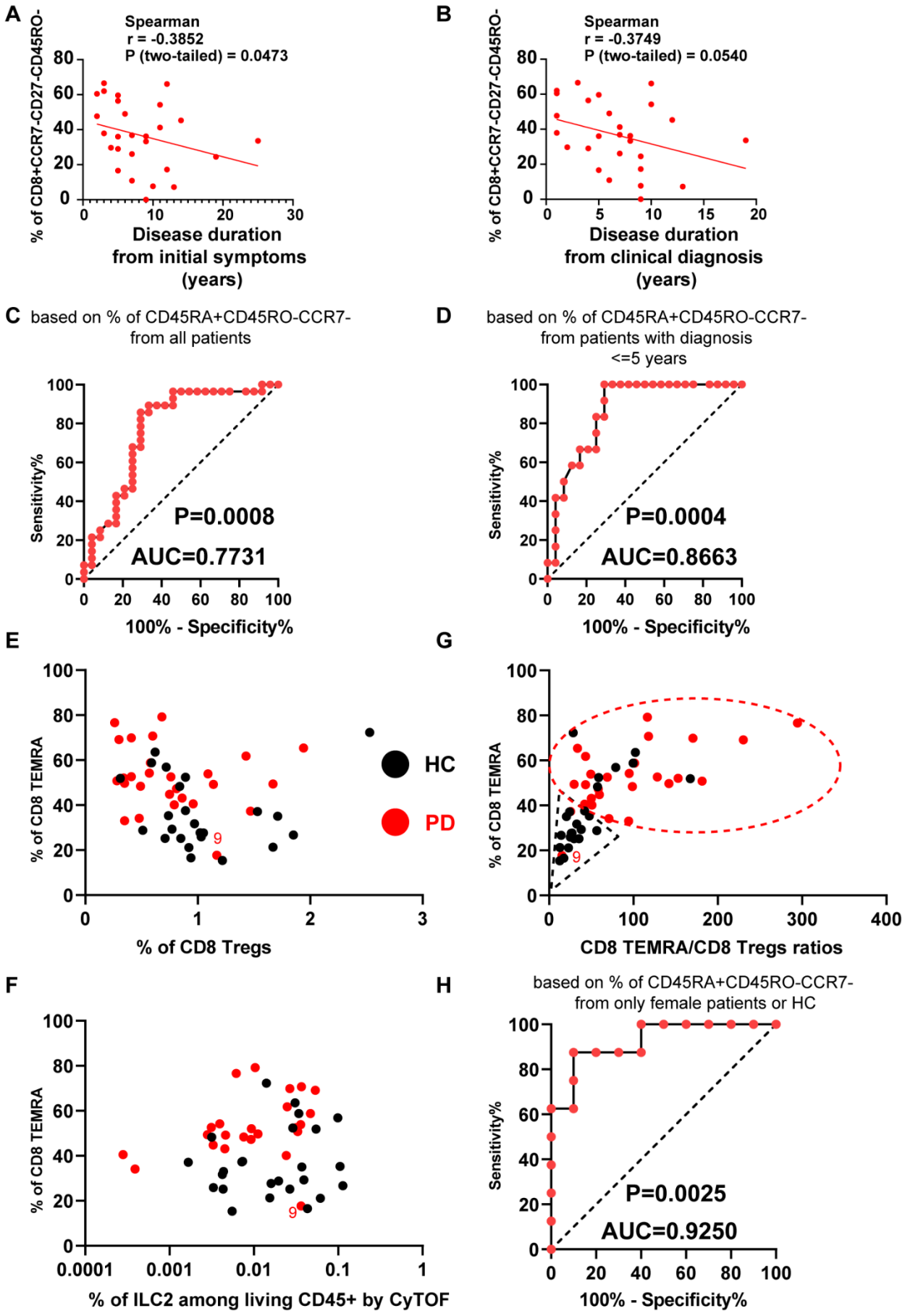
A
Spearman
r = -0.3852
P (two-tailed) = 0.0473
% of CD8+CCR7-CD27-CD45RO-
Disease duration
from initial symptoms
(years)
B
Spearman
r = -0.3749
P (two-tailed) = 0.0540
% of CD8+CCR7-CD27-CD45RO-
Disease duration
from clinical diagnosis
(years)
C
based on % of CD45RA+CD45RO-CCR7-
from all patients
Sensitivity%
100% - Specificity%
P=0.0008
AUC=0.7731
D
based on % of CD45RA+CD45RO-CCR7-
from patients with diagnosis
<=5 years
Sensitivity%
100% - Specificity%
P=0.0004
AUC=0.8663
E
% of CD8 TEMRA
% of CD8 Tregs
HC
PD
G
% of CD8 TEMRA
CD8 TEMRA/CD8 Tregs ratios
F
% of CD8 TEMRA
% of ILC2 among living CD45+ by CyTOF
H
based on % of CD45RA+CD45RO-CCR7-
from only female patients or HC
Sensitivity%
100% - Specificity%
P=0.0025
AUC=0.9250

943

Figure 5. CD8 TEMRA is a reliable easily-accessible cellular biomarker for early iPD.

(**A, B**) Graphs showing the correlation between the frequency of CD8 TEMRA among total CD8 T cells and the disease duration from the onset of initial symptoms (**A**) or from clinical diagnosis (**B**). Correlation coefficient and P-value were calculated based on Spearman correlation. (**C, D**) ROC analysis based on the frequency of $CD45RA^{+}CD45RO^{-}CCR7^{-}$ among total CD8 T cells, yielding an AUC of 0.7731 or 0.8663 for all the early-to-mid stage PD (n=28) (**C**) or patients diagnosed within 5 years (n=12 for diagnosed <=5 years) (**D**) versus all the HC (n=24), respectively. (**E**) Plot showing the frequency of CD8 TEMRA versus the frequency of CD8 Tregs for each individual participant. (**F)** Plot showing the frequency of CD8 TEMRA quantified by flow cytometry versus the frequency of ILC2 quantified by CyTOF for each individual participant. (**G)** Plot showing the frequency of CD8 TEMRA versus the ratios between CD8 TEMRA and CD8 Tregs for each individual. The dashed circle or triangle highlights the PD- or HC-dominant area. (**H**) ROC analysis based on the frequency of $CD45RA^{+}CD45RO^{-}CCR7^{-}$ among total CD8 T cells only from female PD (n=8) or HC (n=10). Each symbol represents the measurement from one individual participant. All the PD (n=28) and HC (n=24) were used in the analysis unless specified. The label “9” was used to highlight the same outlier “PD9” in several plots, which even cannot be distinguished from HC based on all the analysed T-cell features as shown in **Figure 3**. ROC, Receiver operating characteristic; AUC, Area under the curve; HC, healthy controls; PD, patients with Parkinson’s disease.

Supplemental Figures and Legends

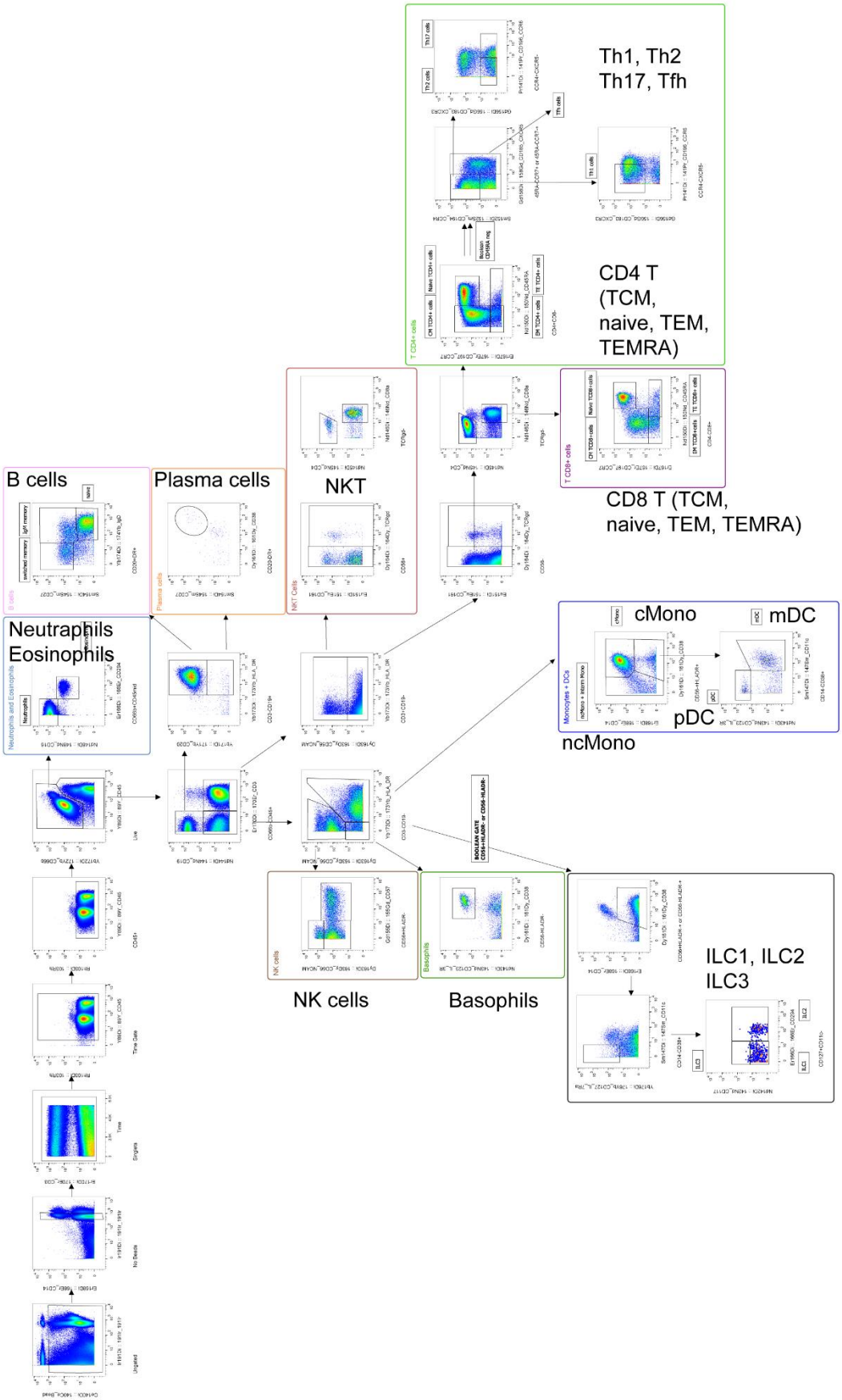

968

969 **Figure S1. CyTOF gating strategy used in this study.**

The gating stategy of the CyTOF analysis for various peripheral immune cells from whole blood. The markers used in this study are provided in **Table S3**. Labels for some of the major subsets are enlarged.

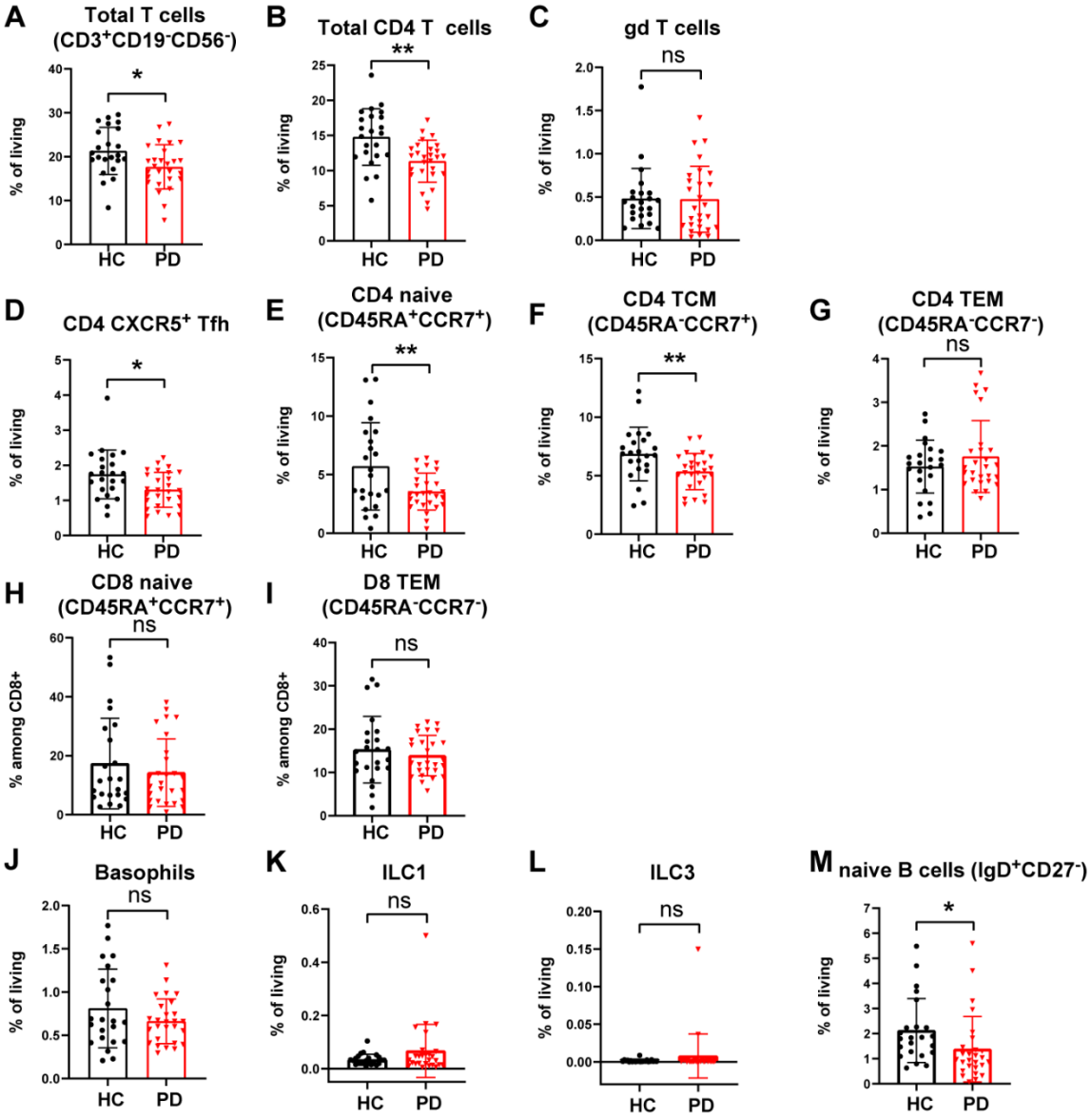

Figure S2. Extended analysis on major immune subsets examined by CyTOF.

(**A-C**) Scatter dot plots showing the frequency of total CD3+ T cells ($CD3^+CD19^-CD56^-$) (**A**), total CD4 T cells (**B**) and γδ T cells (**C**) among living $CD45^+$ cells in PD and HC, as analysed by CyTOF. (**D-G**) Scatter dot plots showing the frequency of circulating CD4 CXCR5+ T follicular help (Tfh) (**D**), CD45RA+CCR7+ naïve (**E**), CD45RA-CCR7+ central memory (TCM) (**F**) and CD45RA-CCR7- effector memory (TEM) (**G**) T cells. (**H, I**) Scatter dot plots showing the frequency of CD45RA+CCR7+ naïve (**H**) and CD45RA-CCR7-effector memory (TEM) (**I**) CD8 T cells. (**J-L**) Scatter dot plots showing the frequency of basophils (**J**), ILC1 (**K**) and ILC3 (**L**) among living $CD45^+$

immune cells. For detailed gating strategy, please refer to **Fig. S1**. (**M**) Scatter dot plots showing the frequency of naïve B cells among living $CD45^+$ immune cells. All the results of major immune subsets were also provided in **Table S5**. The results were analysed using an unpaired two-tailed Student *t* test. Data are presented as mean of the given group± standard deviation (s.d.). Each symbol represents the measurement from one individual participant (**A-M**). ns, not significant; *p<=0.05, **p<=0.01, and ***p<=0.001. HC, healthy controls; PD, patients with Parkinson's disease.

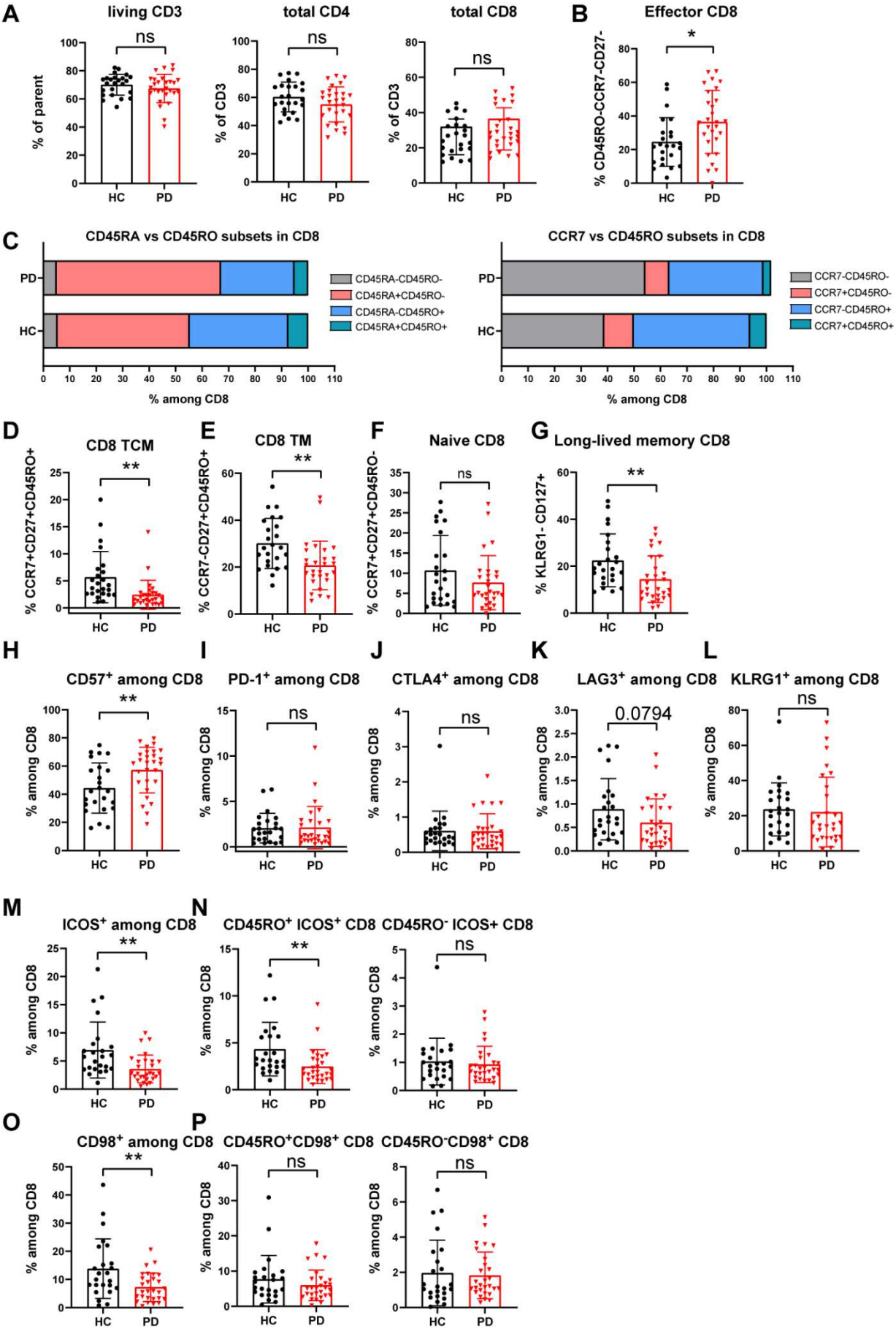
A
living CD3
total CD4
total CD8
B
Effector CD8
% of parent
% of CD3
% CD45RO-CCR7-CD27-
ns
*
HC
PD
C
CD45RA vs CD45RO subsets in CD8
CCR7 vs CD45RO subsets in CD8
CD45RA-CD45RO-
CD45RA+CD45RO-
CD45RA-CD45RO+
CD45RA+CD45RO+
CCR7-CD45RO-
CCR7+CD45RO-
CCR7-CD45RO+
CCR7+CD45RO+
% among CD8
D
CD8 TCM
E
CD8 TM
F
Naive CD8
G
Long-lived memory CD8
% CCR7+CD27+CD45RO+
% CCR7-CD27+CD45RO+
% CCR7+CD27+CD45RO-
% KLRG1- CD127+
**
H
CD57+ among CD8
I
PD-1+ among CD8
J
CTLA4+ among CD8
K
LAG3+ among CD8
L
KLRG1+ among CD8
0.0794
% among CD8
M
ICOS+ among CD8
N
CD45RO+ ICOS+ CD8
CD45RO- ICOS+ CD8
O
CD98+ among CD8
P
CD45RO+CD98+ CD8
CD45RO-CD98+ CD8

988

Figure S3. Early-to-mid iPD show fewer memory CD8 T cells and display no sign of accelerated exhaustion.

(**A**) Scatter dot plots showing the frequency of total CD3+, CD4+ and CD8+ T cells in PD and HC as analysed by FCM. The parent gate of CD3+ cells is living lymphocyte singlets. (**B**) Scatter dot plots showing the frequency of effector CD8 T cells among total CD8 T cells. (**C**) Bar graphs showing the relative average proportions of CD45RA versus CD45RO (left) and CCR7 versus CD45RO quartered subpopulations (right) of CD8 T cells. (**D-G**) Scatter dot plots showing the frequency of TCM (central memory) (**D**), TM (transitional memory) (**E**), naïve (**F**) and long-lived memory (**G**) CD8 T cells in PD and HCs. The combination of markers used to define the corresponding subset was directly described in the title of y axis. (**H-L**) Scatter dot plots showing the frequency of $CD57^+$ (**H**), $PD\text{-}1^+$ (**I**), $CTLA4^+$ (**J**), $LAG3^+$ (**K**) and $KLRG1^+$ (**L**) populations among CD8 T cells in PD and HC. (**M, N**) Scatter dot plots showing the frequency of $ICOS^+$ cells (**M**), $ICOS^+CD45RO^+$ or $ICOS^+CD45RO^-$ cells (**N**) among total CD8 T cells in PD and HC. (**O, P**) Scatter dot plots showing the frequency of $CD98^+$ populations (CD98: amino acid transporter) (**O**) as well as $CD98^+CD45RO^+$ or $CD98^+CD45RO^-$ cells (**P**) among total CD8 T cells. The results were analysed using an unpaired two-tailed Student *t* test. Data are presented as mean of the given group± standard deviation (s.d.). Each symbol represents the measurement from one individual participant (**A, B, D-P**). ns, not significant; *p<=0.05, **p<=0.01, and ***p<=0.001. HC, healthy controls; PD, patients with Parkinson's disease.

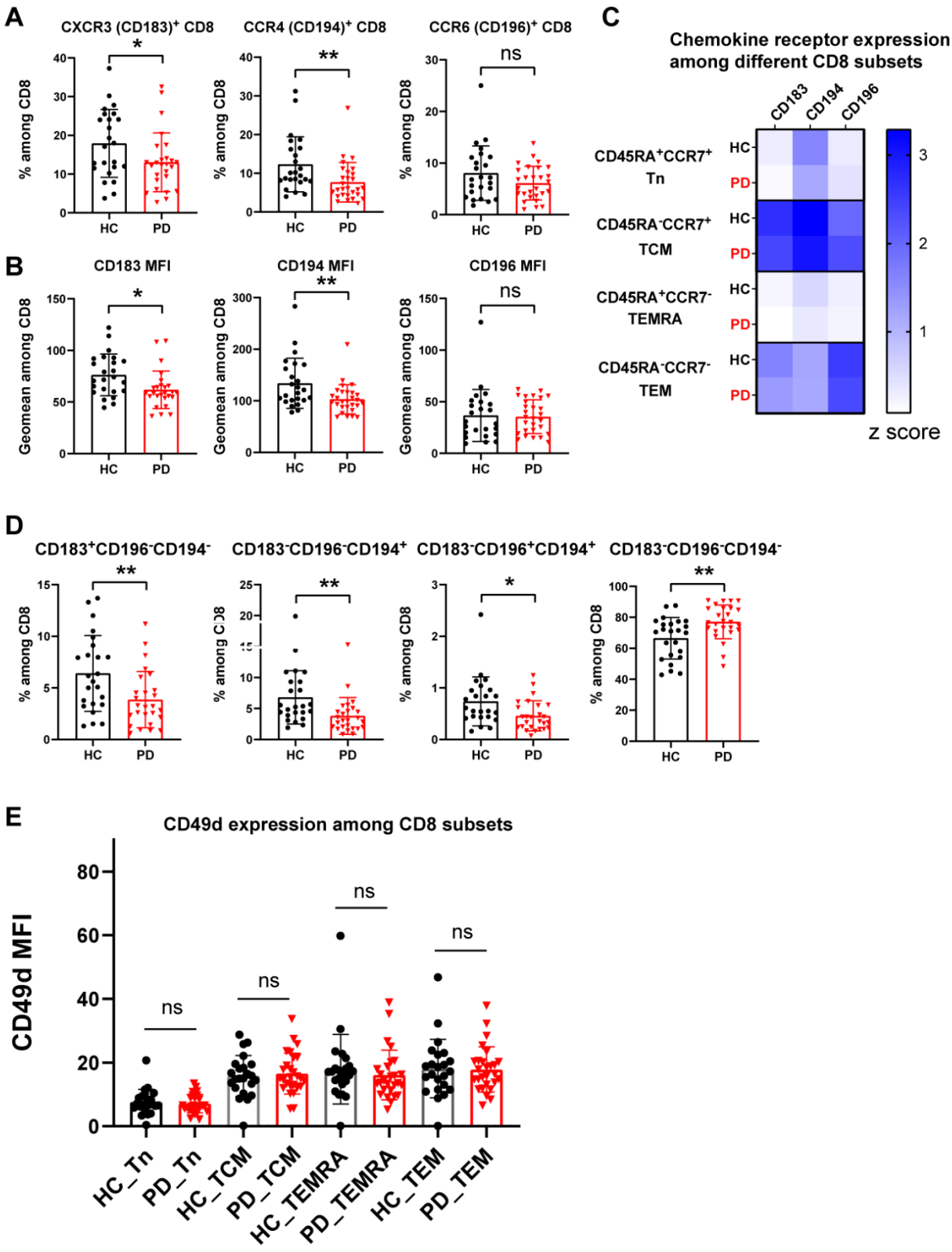

Figure S4. CD8 TEMRA show normal expression of major chemokine receptors and CD49d in early-to-mid iPD.

(**A**) Scatter dot plots showing the frequency of CXCR3/CD183, CCR4/CD194 and CCR6/CD196 positive cells among total CD8 T cells. (**B**) Scatter dot plots showing the geometric mean (geomean,

reflecting MFI) of CXCR3, CCR4 and CCR6 among total CD8 T cells. (**C**) Heatmap showing the averaged expression levels of the analysed chemokine receptors in different subpopulations of CD8 T cells for the given group. The frequency of cells expressing the given chemokine receptor was normalized along column. CCR7 expression was not shown because CCR7 was used to define CD8 memory/naïve T cell subsets. (**D**) Scatter dot plots showing the frequency of CD8 T cells expressing different combinations of the chemokine receptors CXCR3/CD183, CCR4/CD194 and CCR6 /CD196 in PD and HC. (**E**) Scatter dot plots showing the expression level (MFI) of the brain homing factor CD49d among different CD8 T-cell subsets in PD and HC. The results were analysed using an unpaired two-tailed Student *t* test. Data are presented as mean of the given group± standard deviation (s.d.). Each symbol represents the measurement from one individual participant (**A, B, D, E**). ns, not significant; *p<=0.05, **p<=0.01, and ***p<=0.001. HC, healthy controls; PD, patients with Parkinson's disease. Of note, the CD49d expression was analysed by CyTOF while the expression of the chemokine receptors was done using flow cytometry.

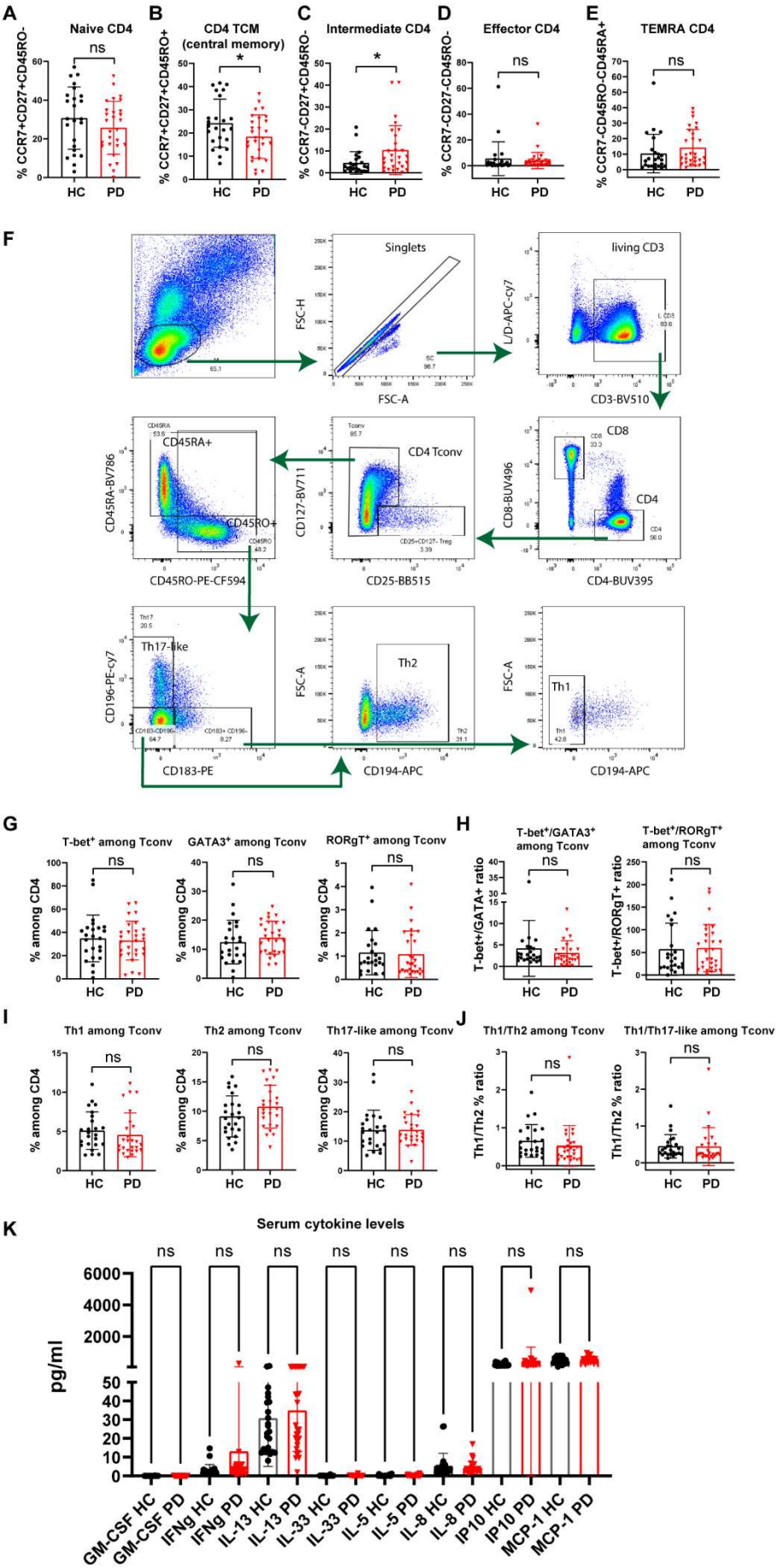
A
Naive CD4
% CCR7+CD27+CD45RO-
ns
HC
PD
B
CD4 TCM (central memory)
% CCR7+CD27+CD45RO+
*
C
Intermediate CD4
% CCR7-CD27+CD45RO-
*
D
Effector CD4
% CCR7-CD27-CD45RO-
ns
E
TEMRA CD4
% CCR7-CD45RO-CD45RA+
ns
F
Singlets
FSC-H
FSC-A
living CD3
L/D-APC-cy7
CD3-BV510
CD4 Tconv
CD127-BV711
CD25-BB515
CD8
CD4
CD8-BUV496
CD4-BUV395
CD45RA+
CD45RO+
CD45RA-BV786
CD45RO-PE-CF594
Th17-like
CD196-PE-cy7
CD183-PE
Th2
CD194-APC
Th1
G
T-bet+ among Tconv
GATA3+ among Tconv
RORgT+ among Tconv
% among CD4
H
T-bet+/GATA3+ among Tconv
T-bet+/GATA3+ ratio
T-bet+/RORgT+ among Tconv
T-bet+/RORgT+ ratio
I
Th1 among Tconv
Th2 among Tconv
Th17-like among Tconv
J
Th1/Th2 among Tconv
Th1/Th2 % ratio
Th1/Th17-like among Tconv
K
Serum cytokine levels
pg/ml
GM-CSF HC
GM-CSF PD
IFNg HC
IFNg PD
IL-13 HC
IL-13 PD
IL-33 HC
IL-33 PD
IL-5 HC
IL-5 PD
IL-8 HC
IL-8 PD
IP10 HC
IP10 PD
MCP-1 HC
MCP-1 PD

1026

Figure S5. CD4 TCM is reduced while CD4 T-helper subset balance is unaffected in early-to-mid iPD.

(**A-E**) Scatter dot plots showing the frequency of naïve (**A**), TCM (central memory) (**B**), intermediate (**C**), effector (**D**) and TEMRA (**E**) CD4 T cells in PD and HC. (**F**) Gating strategy to define CD4 Th1, Th2 and Th17 subsets based on the combinations of the expression of the chemokine receptors CXCR3/CD183, CCR4/CD194, CCR6/CD196 and CCR7/CD197 in PD and HC using flow cytometry analysis. Arrows indicate the workflow. (**G**) Scatter dot plots showing the expression of the master transcriptions factor of CD4 T helper subset Tbet, GATA3 or RORγT in PD and HC. (**H**) Ratios between T-bet$^+$/GATA3$^+$ and T-bet$^+$/RORγT$^+$ CD4 T cells in PD and HC, reflecting the ratios of Th1/Th2 and Th1/Th17, respectively. (**I**) Scatter dot plots showing the frequency of Th1 (CXCR3$^+$CCR6$^-$CCR4$^-$), Th2 (CXCR3$^-$CCR6$^-$CCR4$^+$) and Th17-like (CXCR3$^-$CCR6$^+$) cells based on the combinations of the expression of the chemokine receptors CXCR3, CCR4, CCR6 and CCR7. Of note, the Th17-like data is also similar to our CyTOF data based on the more-strict Th17 gating strategy (CD45RA$^-$CCR4$^+$CCR6$^+$CXCR3$^-$CXCR5$^-$). (**J**) Ratios of Th1/Th2 and Th1/Th17 cells in PD and HC. The ratios in **J** were calculated based on data of **I**. (**K**) Serological levels of analyzed cytokines/chemokines in PD and HC. The results were analysed using an unpaired two-tailed Student *t* test (**A-E, G-J**) or using Brown-Forsythe and Welch ANOVA test with Dunnette's T3 multiple comparison test (**K**). Data are presented as mean of the given group± standard deviation (s.d.). Each symbol represents the measurement from one individual participant (**A-E**, **G-J, K**). ns, not significant; *p<=0.05, **p<=0.01, and ***p<=0.001. HC, healthy controls; PD, patients with Parkinson's disease.

Supplemental Tables

Table S1. The exclusion criteria of the cohort.

Exclusion Criteria	
History or presence of medication taken	Corticosteroids Cytostatic drugs Immunosuppressive treatment Iodine*
Medical history	Autoimmune Disorders Chronic Infections Endocrine Diseases Gastrointestinal Diseases Haematological Diseases Immunodeficiency Malignancies Neurologic Diseases (other than Parkinson's disease)

* Iodine treatment could interfere with the mass cytometry (CyTOF) staining and was therefore excluded.

Table S2. Basic demographics and clinical information of the participants in the cohort.

	Parkinson's cases (n=28)	**Controls (n=24)**	**P-value**
Male, % (n)	68 (19)	58 (14)	0.17 (Chi square test)
Age at basic assessment, mean (SD)[£]	64.9 (6.97)	63.92(3.75)	0.54 (two-tailed Student *t* test)
Age of Onset, mean (SD)	58.14 (9.42)	NA	NA
Disease duration from diagnosis (years), mean (SD)	6.64 (4.12)	NA	NA
Disease duration from initial symptom(s), mean (SD)	8.19 (5.37)	NA	NA
Family History of Parkinson's Disease, % (n)	43 (12)	NA	NA
Hoehn and Yahr (H&Y) Staging scale, mean (SD)	2.3 (0.42)	NA	NA
UPDRS-III*, mean (SD)	39.69 (13.15)	NA	NA
LEDD[¥], mean (SD)	610.58 (344.06)	NA	NA
MOCA[€], mean (SD)	25.21 (3.82)	NA	NA

£, descriptive statistics here includes information from all idiopathic and three genetic PD.
*UPDRS-III: Motor Examination. The physician does a number of tests to rate the cardinal symptoms of PD such as rigidity, postural instability, facial expression etc.
¥LEDD: Levodopa Equivalent Daily Dose, so basically the sum of levodopa a patient is taking each day.
€MOCA: Montreal Cognitive Assessment. Provides an overall cognitive profile (0-30, with 30 meaning no cognitive deficits).
NA, no data available or not applicable; SD, standard deviation.

Table S3. Mass Cytometry (CyTOF) antibodies used to stain the whole blood.

Metal Isotope	Antibody	Clone	Manufacturer	Catalogue#
89Y	CD45	HI30	Fluidigm	Part of MDIPA
103Rh	Live/Dead indicator		Fluidigm	Part of MDIPA
141Pr	CD196 (CCR6)	G034E3	Fluidigm	Part of MDIPA
142Nd	CD117 (c-kit)*	104D2	Biolegend	313223
143Nd	CD123	6H6	Fluidigm	Part of MDIPA
144Nd	CD19	HIB19	Fluidigm	Part of MDIPA
145Nd	CD4	RPA-T4	Fluidigm	Part of MDIPA
146Nd	CD8a	RPA-T8	Fluidigm	Part of MDIPA
147Sm	CD11c	Bu15	Fluidigm	Part of MDIPA
148Nd	CD16	3G8	Fluidigm	Part of MDIPA
149Sm	CD45RO	UCHL1	Fluidigm	Part of MDIPA
150Nd	CD45RA	HI100	Fluidigm	Part of MDIPA
151Eu	CD161	HP-3G10	Fluidigm	Part of MDIPA
152Sm	CD194 (CCR4)	L291H4	Fluidigm	Part of MDIPA
153Eu	CD25	BC96	Fluidigm	Part of MDIPA
154Sm	CD27	O323	Fluidigm	Part of MDIPA
155Gd	CD57	HCD57	Fluidigm	Part of MDIPA
156Gd	CD183 (CXCR3)	G025H7	Fluidigm	Part of MDIPA
158Gd	CD185 (CXCR5)	J252D4	Fluidigm	Part of MDIPA
159Tb	KLRG1*	SA231A2	Biolegend	367702
160Gd	CD28	CD28.2	Fluidigm	Part of MDIPA
161Dy	CD38	HB-7	Fluidigm	Part of MDIPA
162Dy	CD336 (NKp44)*	P44-8	Biolegend	325102
163Dy	CD56 (NCAM)	NCAM16.2	Fluidigm	Part of MDIPA
164Dy	TCRgd	B1	Fluidigm	Part of MDIPA
165Ho	CD223 (LAG3)	11C3C65	Fluidigm	3165037B

166Er	CD294	BM16	Fluidigm	Part of MDIPA
167Er	CD197 (CCR7)	G043H7	Fluidigm	Part of MDIPA
168Er	CD14	63D3	Fluidigm	Part of MDIPA
169Tm	CD49d*	9F10	Biolegend	304302
170Er	CD3	UCHT1	Fluidigm	Part of MDIPA
171Yb	CD20	2H7	Fluidigm	Part of MDIPA
172Yb	CD66b	G10F5	Fluidigm	Part of MDIPA
173Yb	HLA-DR	LN3	Fluidigm	Part of MDIPA
174Yb	IgD	IA6-2	Fluidigm	Part of MDIPA
175Lu	CD279 (PD1)	EH12.2H7	Fluidigm	3175008B
176Yb	CD127	A019D5	Fluidigm	Part of MDIPA

* in house conjugation using Maxpar X8 Antibody Labeling Kits MDIPA (201325, Fluidigm)

Table S4. Flow cytometry antibodies used to stain the PBMCs of participants analysed in this study.

Ab Target	Fluorochrome	Dilution	Manufacturer	Reference	Clone
Fc Blocking Abs	/	1:50	BD	564765	/
CD3*	BUV737	1:100	BD	741822	HIT3a
CD3*	BV510	1:100	BD	564713	HIT3a
CD4	BUV395	1:100	BD	563550	SK3
CD8	BUV496	1:100	BD	564804	RPA-T8
CD25	BV786	1:50	BD	741035	2A3
CD25	BB515	1:50	BD	564467	2A3
CD27	BB700	1:50	BD	566450	M-T271
CD28	BUV785	1:50	BioLegend	302950	CD28.2
CD31	BV605	1:50	BD	562855	WM59
CD39	BV711	1:50	BioLegend	328228	A1
CD45RA	BV421	1:50	BioLegend	304130	HI100

CD45RA	BV785	1:50	BioLegend	304140	HI100
CD45RO	PE-CF594	1:50	BD	562299	UCHL1
CD57	FITC	1:50	BD	555619	NK-1
CD71	FITC	1:50	BioLegend	334104	CY1G4
CD98	BV786	1:50	BD	744507	UM7F8
CD122	PE	1:50	BioLegend	339006	TU27
CD127 (IL7R)	BV421	1:50	BD	562436	HIL-7R-M21
CD127 (IL7R)	BV711	1:50	BioLegend	351328	A019D5
CD183 (CXCR3)	PE	1:50	BD	560928	1C6/CXCR3
CD194 (CCR4)	APC	1:50	BioLegend	359408	L291H4
CD196 (CCR6)	PE-Cy7	1:50	BD	560620	11A9
CD197 (CCR7)	BV421	1:50	BioLegend	353208	G043H7
CD223 (LAG3)	BV711	1:50	BioLegend	369320	11C3C65
CD278 (ICOS)	BV605	1:50	BioLegend	313538	C398.4A
CD279 (PD-1)	BV605	1:50	BioLegend	329924	EH12.2H7
GLUT1	PE	1:500	Abcam	ab209449	EPR3915
KLRG1	PE-Cy7	1:50	BioLegend	368614	14C2A07
Intracellular markers					
CD152 (CTLA4)	PE-Cy5	1:20	BD	555854	BNI3
FOXP3	APC	1:20	BioLegend	320114	206D
Phospho S6	AF488	1:20	CST	4803S	D57.2.2E
Helios	Pacific Blue	1:20	BioLegend	137220	22F6
Ki-67	FITC	1:20	BD	561165	B56
GATA3	PE-Cy7	1:20	BD	560405	L50-823

RORγT	BV650	1:20	BD	563424	Q21-559
T-bet	PE	1:20	BioLegend	644810	4B10
Eomes	PE-Cy7	1:20	Thermo Fisher Scientific	25-4877-42	WD1928
Live/Dead	APC-Cy7	1:500	Thermo Fisher Scientific	L34976	/

*, different flurorochromes might be used in different staining panels as we employed five staining panels in parallel.

Table S5. Mass cytometry analysis reveals the percentages of major immune subsets among living CD45+ singlets or among the relevant parent gates (Fig S1) in the peripheral blood of early-to-mid stage iPD patients or matched healthy controls aged 60-70 years.

No.	Items	HC (n=24), mean (SD)	PD (n=28), Mean (SD)	P-value (two-tailed t test)
	Total number of living CD45+ singlets	627629 (136842)	679999 (155232)	0.22482
	Among living CD45+ singlets			
1	ncMono plus interm Mono among living cells	0.847 (0.518)	0.75 (0.422)	0.476922
2	mDC among living cells	0.253 (0.065)	0.215 (0.07)	0.062098
3	pDC among living cells	0.111 (0.04)	0.097 (0.04)	0.24072
4	cMono among living cells	5.964 (1.085)	5.913 (1.37)	0.887997
5	Basophils among living cells	0.81 (0.445)	0.662 (0.253)	0.154289
6	NK among living cells	3.658 (1.6)	3.53 (1.747)	0.794596
7	$CD56^{high}CD57^{-}$ immature NK among living cells	0.224 (0.131)	0.16 (0.088)	0.04992
8	$CD56^{mid}CD57^{-}$ NK among living cells	1.619 (0.78)	1.549 (0.989)	0.788334
9	$CD56^{mid}CD57^{+}$ late NK among living cells	1.815 (1.174)	1.823 (1.181)	0.982319
10	Total ILCs among living cells	0.069 (0.042)	0.091 (0.127)	0.419163
11	ILC1 among living cells	0.034 (0.021)	0.067 (0.098)	0.123848
12	ILC2 among living cells	0.033 (0.033)	0.017 (0.015)	0.025059
13	ILC3 among living cells	0.001 (0.002)	0.008 (0.029)	0.290684
14	B cells among living cells	3.24 (1.419)	3.453 (3.736)	0.801529

15	$CD27^{+}CD38^{+}$ plasma cells among living cells	0.02 (0.021)	0.015 (0.01)	0.313471
16	$CD20^{-}HLADR^{+}$ among living cells	0.12 (0.37)	0.62 (2.09)	0.270256
17	$CD20^{+}HLADR^{+}$ among living cells	3.082 (1.363)	2.731 (3.217)	0.635057
18	$CD27^{-}IgD^{+}$ naïve B cells among living cells	2.12 (1.25)	1.379 (1.282)	0.04885
19	$CD27^{+}IgD^{-}$ class-switched memory B among living cells	0.395 (0.226)	0.385 (0.368)	0.911043
20	$CD27^{+}IgD^{+}$ IgM memory among living cells	0.39 (0.253)	0.781 (2.146)	0.39954
21	Total T cells among living cells	21.318 (5.235)	17.673 (4.946)	0.016814
22	$TCRgd^{-}$ classic T cells among living cells	20.835 (5.119)	17.198 (4.728)	0.013785
23	CD8+ T among living cells	5.42 (2.514)	5.372 (2.671)	0.950139
24	$CD45RA^{-}CCR7^{-}$ CD8 TEM among living cells	0.795 (0.453)	0.748 (0.43)	0.712639
25	$CD45RA^{-}CCR7^{+}$ CD8 CM among living cells	1.528 (0.963)	0.955 (0.536)	0.012486
26	$CD45RA^{+}CCR7^{-}$ CD8 TEMRA among living cells	2.165 (1.829)	2.839 (2.109)	0.247063
27	$CD45RA^{+}CCR7^{+}$ CD8 naïve T among living cells	0.783 (0.567)	0.72 (0.613)	0.713217
28	$CD4^{+}$ among living cells	14.776 (3.947)	11.321 (2.945)	0.001126
29	$CD45RA^{-}$ CD4 among living cells	8.371 (2.389)	7.099 (1.927)	0.046814
30	CD4 CXCR3+CCR6-CCR4-CXCR5- Th1 among living cells	1.829 (0.745)	1.636 (0.958)	0.443708
31	CD4 CXCR3-CCR6-CCR4+CXCR5- Th2 among living cells	1.246 (0.535)	1.01 (0.41)	0.090831
32	CD4 CXCR3-CCR6+CCR4+CXCR5- Th17 among living cells	0.519 (0.319)	0.549 (0.329)	0.749899
33	CD4 CXCR5+Tfh among living cells	1.741 (0.678)	1.304 (0.485)	0.012681
34	$CD45RA^{-}CCR7^{-}$ CD4 T among living cells	1.527 (0.594)	1.756 (0.81)	0.276958
35	$CD45RA^{-}CCR7^{+}$ CD4 T among living cells	6.848 (2.238)	5.345 (1.518)	0.008301
36	$CD45RA^{+}CCR7^{-}$ CD4 T among living cells	0.547 (0.598)	0.566 (0.647)	0.91715
37	$CD45RA^{+}CCR7^{+}$ CD4 T among living cells	5.699 (3.643)	3.55 (1.543)	0.00885
38	$TCRgd^{+}$ T among living cells	0.483 (0.341)	0.475 (0.376)	0.943847
39	NKT among living cells	2.407 (2.604)	2.431 (1.738)	0.969286
40	$CD8^{+}$ NKT among living cells	1.33 (1.146)	1.722 (1.345)	0.287332
41	$CD4^{+}$ NKT among living cells	0.973 (1.737)	0.546 (0.869)	0.27652
42	Eosinophils among living cells	2.682 (1.914)	1.628 (1.005)	0.018555
43	Neutrophils among living cells	54.853 (13.872)	62.153 (8.156)	0.028426

	Among parent gate			
44	ncMono plus interm Mono among CD3-CD19-CD56-+HLADR+	11.35 (5.243)	10.469 (4.895)	0.550335
45	cDC among $CD14^{-}CD38^{+}$	58.174 (5.712)	56.277 (9.996)	0.434193
46	pDC among $CD14^{-}CD38^{+}$	25.269 (6.242)	25.391 (8.386)	0.955228
47	cMono among $CD56^{-+}HLADR^{+}$	82.436 (5.429)	83.938 (5.407)	0.343294
48	Basophils among $CD56^{-}HLADR^{-}$	58.465 (18.293)	55.279 (15.374)	0.515111
49	NK among $CD3^{-}CD19^{-}$	28.807 (8.605)	28.745 (10.793)	0.982812
50	$CD56^{high}CD57^{-}$ immature NK among NK	7.04 (4.954)	6.009 (5.045)	0.47997
51	$CD56^{mid}CD57^{-}$ among NK	46.359 (13.894)	43.532 (15.477)	0.511909
52	$CD56^{mid}CD57^{+}$ late NK among NK	46.593 (16.195)	50.501 (16.552)	0.414395
53	Total ILCs among $CD14^{-}CD38^{+}$	1.831 (1.191)	2.776 (3.886)	0.276966
54	ILC1 among ILCs	56.917 (22.262)	67.578 (21.7)	0.100179
55	ILC2 among ILCs	40.648 (23.368)	28.852 (22.595)	0.082335
56	ILC3 among ILCs	2.447 (3.122)	3.641 (5.285)	0.356174
57	CD19 B cells among $CD66b^{-}CD45^{+}$	8.33 (3.671)	9.264 (8.883)	0.646487
58	$CD20^{-}HLADR^{+}$ among B cells	2.966 (7.355)	7.78 (20.574)	0.301677
59	$CD27^{+}CD38^{+}$ plasma cells among $CD20^{-}$ $HLADR^{+}$ B cells	40.636 (23.249)	41.301 (22.297)	0.919915
60	$CD20^{+}HLADR^{+}$ among B cells	95.712 (7.352)	90.113 (22.339)	0.265394
61	$CD27^{-}IgD^{+}$ naïve among $CD20^{+}HLADR^{+}$	66.453 (14.11)	54.928 (20.903)	0.032729
62	$CD27^{+}IgD^{-}$ class-switched memory among $CD20^{+}HLADR^{+}$	13.723 (6.809)	17.912 (9.271)	0.085198
63	$CD27^{+}IgD^{+}$ IgM memory among $CD20^{+}HLADR^{+}$	13.893 (8.827)	17.886 (16.107)	0.303826
64	$CD56^{-}$ among $CD3^{+}CD19^{-}$	89.615 (7.828)	86.881 (6.587)	0.19508
65	$TCRgd^{-}$ classic T cells among total T cells	97.757 (1.451)	97.493 (1.734)	0.574621
66	$CD4^{-}CD8^{+}$ among classic T cells	25.705 (9.137)	30.118 (9.619)	0.1116
67	$CD45RA^{-}CCR7^{-}$ TEM among CD8	15.245 (7.516)	13.889 (4.561)	0.446601
68	$CD45RA^{-}CCR7^{+}$ CM among CD8	28.582 (11.591)	19.871 (10.181)	0.007914
69	$CD45RA^{+}CCR7^{-}$ TEMRA among CD8	36.179 (17.486)	49.607 (16.594)	0.008928
70	$CD45RA^{+}CCR7^{+}$ naïve among CD8	17.326 (14.998)	14.272 (11.24)	0.424869
71	$CD4^{+}CD8^{-}$ among classic T cells	71.145 (9.198)	66.911 (9.867)	0.132923

72	Th1 among CD4 $CCR4^{-}CXCR5^{-}$	61.282 (16.004)	54.486 (16.115)	0.150608
73	Th2 among CD4 $CCR4^{+}CXCR5^{-}$	35.101 (11.204)	34.506 (11.046)	0.854118
74	Th17 among CD4 $CCR4^{+}CXCR5^{-}$	14.757 (7.026)	18.987 (11.054)	0.127509
75	Tfh among CD4 $CD45RA^{-}$	20.455 (3.61)	18.299 (4.566)	0.079396
76	$CD45RA^{-}CCR7^{-}$ TEM among CD4	12.154 (8.916)	15.618 (5.296)	0.102741
77	$CD45RA^{-}CCR7^{+}$ CM among CD4	47.508 (12.756)	47.847 (9.05)	0.914884
78	$CD45RA^{+}CCR7^{-}$ TEMRA among CD4	4.052 (4.889)	4.934 (5.083)	0.545261
79	$CD45RA^{+}CCR7^{+}$ naïve among CD4	35.278 (16.482)	30.65 (10.146)	0.240098
80	TCRgd^{+} T among $CD56^{-}$	2.24 (1.452)	2.506 (1.736)	0.570601
81	Total NKT among $CD56^{+}$	85.402 (12.74)	83.294 (15.719)	0.616183
82	$CD8^{+}$ NKT among NKT	59.129 (20.227)	70.188 (16.402)	0.041839
83	$CD4^{+}$ NKT among NKT	33.515 (22.057)	20.707 (16.692)	0.026705
84	Eosinophils among $CD66b^{+}CD45^{mid}$	4.529 (3.466)	2.604 (1.61)	0.014893
85	Neutrophils among $CD66b^{+}CD45^{mid}$	90.811 (19.671)	97.055 (1.653)	0.114084
86	$CD27^{+}CD38^{+}$ plasma cells among B cells	0.64 (0.58)	0.91 (1.11)	0.304309
87	$CD27^{-}IgD^{+}$ naive among B cells	64.28 (15.04)	51.7 (23.15)	0.033506
88	$CD27^{+}IgD^{-}$ class-switched among B cells	12.74 (4.82)	15.03 (8.13)	0.252162
89	$CD27^{+}IgD^{+}$ IgM memory among B cells	13.01 (7.8)	15.6 (15.92)	0.489398

1090